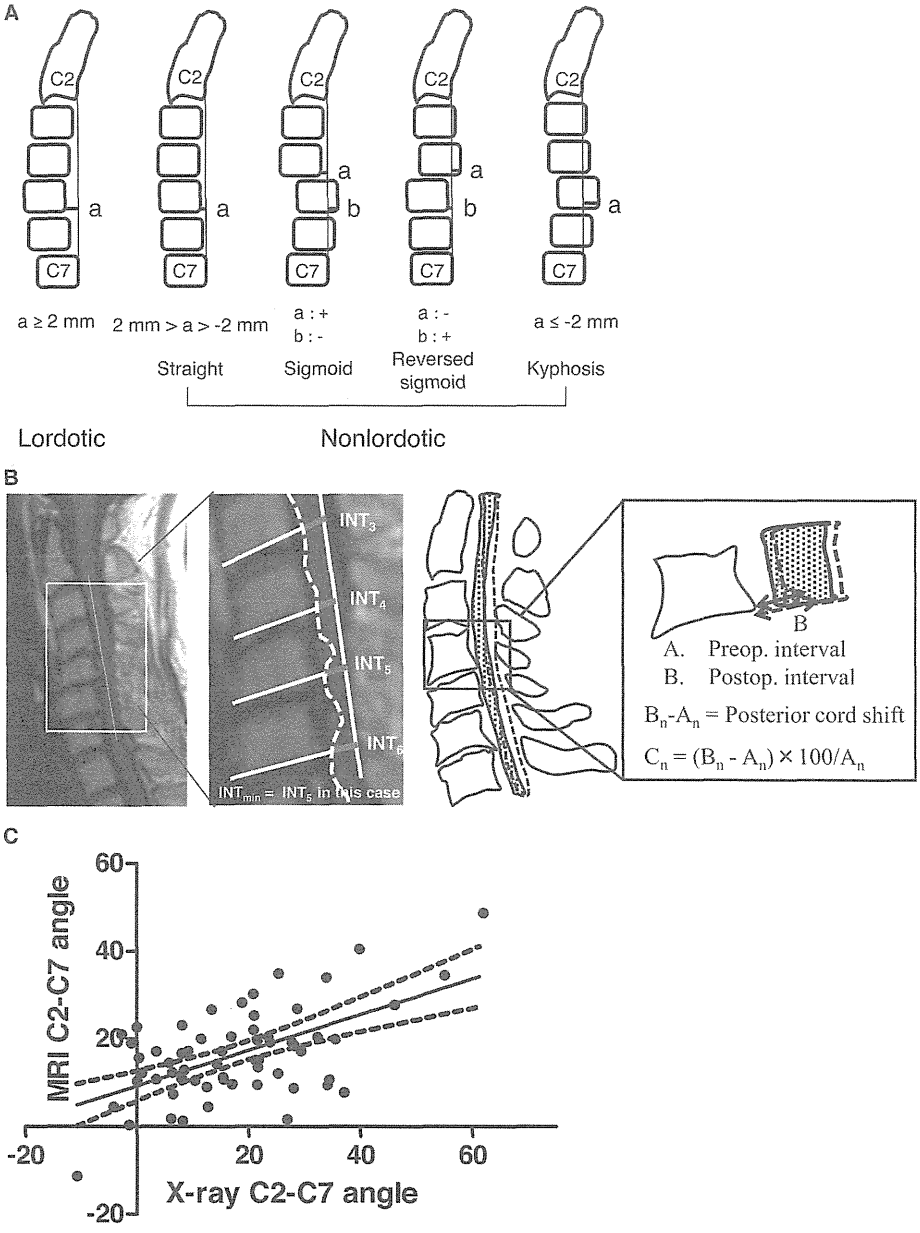

Figure 1. A, Classification of cervical alignment by Kamata *et al.*[14,15] B, The modified K-line (mK-line) was defined as the line connecting the midpoints of the spinal cord at C2 and C7 on preoperative T1-weighted sagittal magnetic resonance imaging (*left*). The interval (INT_n) between the K-line and the most anterior feature of the spinal canal at each segment was measured (n = 3–6; *center*). The minimum interval between the mK-line and the anterior compression-causing feature of the spinal canal in the midsagittal image was defined as INT_{min} (*center*). The interval between the midpoint of the cord and posterior edge of the anterior factor before and after surgery was measured and then the spinal cord shift at each segment was calculated (*right*). C, A significant correlation between the C2–C7 angle on magnetic resonance imaging and that on radiography was observed in this series ($y = 0.407x + 9.275$, *y*: MRI: C2–C7, *x*: radiography: C2–C7, $r^2 = 0.332$; $P < 0.01$), suggesting that the neck position at which magnetic resonance imaging was obtained was similar to the cervical neutral position. MRI indicates magnetic resonance imaging. Preop indicates preoperative; Postop, postoperative.

modified K-line was defined as a line connecting the midpoint of the spinal cord at C2 (determined at the level of the inferior endplate) to that at C7 on T1-weighted MR image (mK-line; Figure 1B, *left*). This line is different from the K-line that connects the midpoints of the spinal canal at C2 and C7 on the basis of conventional lateral radiography.[19] The interval (INT_n) between the mK-line and the anterior factor of the spinal canal, such as disc bulging or a bony spur, at each segment (n = 3–6) was measured before surgery. The sum of the measured intervals (INT_{sum}) was then calculated for each patient (Figure 1B, *center*). In addition, INT_{min} was defined as the lowest INT_n in each case, as we previously reported[12] (Figure 1B, *center*), and was also collected for each patient. The pre- and postoperative INT_n at each segment from C3 to C6 were measured on sagittal T1-weighted MR image to evaluate the actual migration of the spinal cord, which was defined as $C_n = (B_n - A_n) \times 100/A_n$ (n = 3–6; A_n and B_n represent the preoperative and postoperative INT_n, respectively, Figure 1B, *right*). To evaluate the global posterior migration of the spinal cord, we calculated $C_{sum} = C_3 + C_4 + C_5 + C_6$ and then analyzed the relationship between preoperative INT_n and C_n (n = 3–6) to determine whether the mK-line could predict a postoperative shift in the spinal cord. The presence of signal intensity changes in the cord was also evaluated on sagittal view T2-weighted MR images of each patient. In preoperative radiography, the cervical sagittal alignment (C2–C7 lordotic angle), determined from tangential lines drawn on the posterior edges of the C2 and C7 bodies, was measured on mid-sagittal MRI and on X-rays obtained in the cervical neutral position to determine whether the neck position

on MRI was similar to the cervical neutral neck position on radiography.

Statistical Analysis

Student unpaired *t* test was used to evaluate the differences in each parameter between the lordotic and nonlordotic groups, except for the RR of the JOA score, INT_{sum}, INT_{min}, and C_{sum}, for which the Mann-Whiney *U* test was used. A cross-correlation analysis was used to evaluate the correlation between INT_n and C_n at each segment. A linear regression analysis was used to investigate whether INT_{sum} was correlated to C_{sum} or the RR of the JOA score. All data are expressed as the mean ± SD. *P* value of less than 0.05 was defined as statistically significant.

RESULTS

Sagittal Cervical Alignment Measured by MRI Significantly Correlates With That Measured by Radiography

Prior to investigation of the relationship between the mK-line determined by MRI and the shift in the spinal cord or clinical outcome, we determined whether the sagittal alignment measured by MRI (MRI, C2–C7) agreed with that measured by neutral radiography (C2–C7) in each case. There was a significant correlation between MRI, C2–C7 and radiography, C2–C7 in this series ($y = 0.407x + 9.275$; *y*: MRI, C2–C7; *x*: radiography, C2–C7; $r^2 = 0.332$; $P < 0.01$, Figure 1C). This result suggests that the neck position at which MR image was obtained was similar to the cervical neutral position.

Anticipated Cord Shift Calculated Using the mK-line Significantly Correlates With Actual Posterior Cord Shift

Table 2 shows the values for INT_n and C_n (Figure 1B, *right*) at each segment in all patients (n = 3–6). The maximum interval was 7.3 mm at the C4 level. The average INT_{sum} value was 27.5 mm. Similarly, the maximum posterior cord shift was 30.3% at the C4 level and the average C_{sum} was 99.3%. Cross-correlation analysis demonstrated significant similarity between the waveform distribution of INT_n and that of C_n ($R = 0.889$, $P < 0.05$; Figure 2A).

INT_{sum} Predicts the Posterior Shift of the Spinal Cord in Lordotic But Not in Nonlordotic Patients

There were no significant differences in age, ratio of males, preoperative JOA score, RR of JOA score, posterior shift of the whole spinal cord, positive ratio of the presence of signal intensity changes in the spinal cord, or incidence of C5 palsy between the lordotic and nonlordotic groups (Table 3). However, we found that patients in the lordotic group had a higher preoperative lordosis angle, INT_{sum}, and INT_{min} than patients in the nonlordotic group (Table 3). In addition, INT_{sum} was associated with $\%C_{sum}$ only in the lordotic group ($y = 4.527x - 36.48$, $y = \%C_{sum}$, $x = INT_{sum}$, $r^2 = 0.1333$, $P < 0.05$; Figure 2B); there was no significant correlation between INT_{sum} and C_{sum} in the nonlordotic group (data not shown).

TABLE 2. Interval Between the K-line and the Anterior Feature of the Spinal Canal and the Extent of Actual Posterior Cord Migration at Each Segment*

Segment	Interval (mm)	Ratio of Posterior Cord Shift (C_n)
C3	6.5 ± 2.6	17.9 ± 26.8
C4	7.3 ± 3.1	30.3 ± 31.5
C5	6.9 ± 2.7	28.9 ± 33.9
C6	6.8 ± 2.2	22.2 ± 31.6
Total	INT_{sum} = 27.5 ± 9.0	C_{sum} = 99.3 ± 83.7

**Data are expressed as the mean ± SD.*

INT_{sum} indicates the sum of the intervals between the K-line and the anterior feature of the spinal canal at each segment (C3–C6); C_n: $(B_n - A_n) \times 100/A_n$ ($n = 3–6$; A_n and B_n represent the preoperative and postoperative intervals between the midpoint of the spinal cord and the anterior impingement at each segment from C3 to C6 levels); C_{sum}, the sum of C3, C4, C5, and C6.

INT_{sum} Is Not a Predictive Factor for Postoperative Clinical Outcome After LAMP

To evaluate the relationship between anticipated postoperative cord shift determined from preoperative MRI and clinical outcomes, we analyzed a linear regression model for INT_{sum} and the RR of the JOA score in each group. The linear regression analysis indicated no significant correlation between INT_{sum} and the RR of the JOA score in both groups (data not shown).

INT_{min} Can Predict Clinical Outcome in Nonlordotic Patients

It is important for spine surgeons to predict postoperative clinical outcomes, particularly in patients with cervical misalignment such as kyphotic or sigmoid alignment, before selecting a surgical procedure for the treatment of CSM. As several studies have reported,[20–23] age, duration of symptoms, and the presence of signal intensity changes in the spinal cord observed on T2-weighted sagittal MR image are risk factors for poor outcome after surgical treatment. Although we did not find significant associations between clinical outcome and either age or duration of preoperative symptoms using linear regression models, we observed that the RR in patients older than 75 years was poorer than that in younger patients in both groups (data not shown). In addition, because most of the patients presented high signal intensity changes in the spinal cord on T2-weighted imaging in both the lordotic and nonlordotic groups, we were not able to analyze whether the signal intensity change in the spinal cord was associated with poor clinical outcome in this series.

Next, we focused on INT_{min}, which has been shown to be a powerful tool to predict residual anterior impingement of the spinal cord after LAMP,[12] for potential prediction of postoperative neurological outcome in nonlordotic patients. Although INT_{min} was not associated with the RR of the JOA score in lordotic patients (data not shown), it was significantly

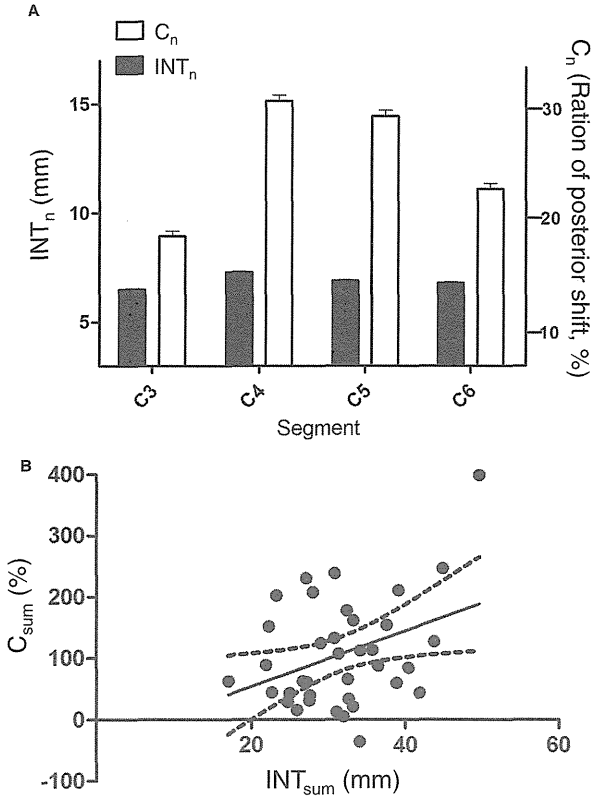

Figure 2. A, The maximum interval was 7.3 mm at the C4 level, and the maximum posterior cord shift was 30.3% at the C4 level. Cross-correlation analysis demonstrated significant similarity between the waveform distribution of INT_n and that of C_n ($R = 0.889$, $P < 0.05$). B, INT_{sum} was significantly correlated with C_{sum} in only the lordotic patient group ($y = 4.527x - 36.48$, $y = C_{sum}$, $x = INT_{sum}$, $r^2 = 0.1333$; $P < 0.05$).

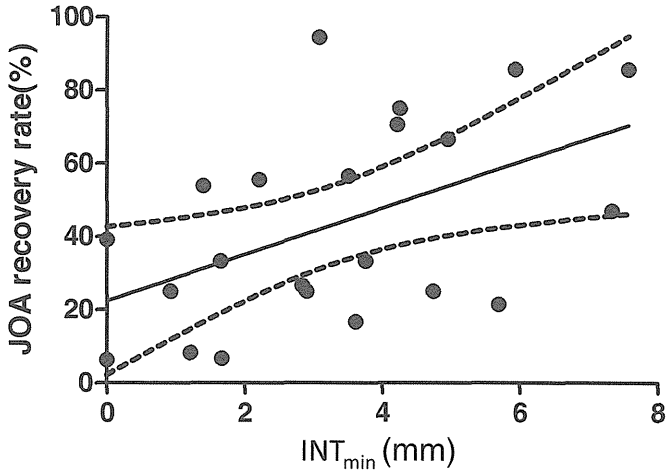

Figure 3. A significant positive correlation between INT_{min} and the recovery rate of the JOA score was confirmed ($y = 6.347x + 22.36$, y = JOA score recovery rate, $x = INT_{min}$, $r^2 = 0.2491$; $P < 0.05$). JOA indicates The Japanese Orthopaedic Association.

and positively correlated with the RR in nonlordotic patients ($y = 6.347x + 22.36$, y = JOA score RR, $x = INT_{min}$, $r^2 = 0.2491$, $P < 0.05$; Figure 3). Based on this analysis, an RR higher than 50% requires INT_{min} of greater than 4.4 mm in nonlordotic patients.

Case Presentation

A 68-year-old male presented with bilateral hand numbness and clumsiness. Preoperative sagittal MR image showed that an anterior feature at the C3–C4 level was related to local kyphosis on sigmoid alignment (Figure 4, *left*). Although he received LAMP for multisegmental stenosis, postoperative compression of the dural sac and anterior spinal cord existed at the C3–C4 level on MR image (Figure 4, *right*). Although INT_{sum} was 22.2 mm, which was higher than the average value in the nonlordotic group, the preoperative INT_{min} was 1.7 mm at the C3–C4 level. The JOA score recovered by 33.3% and the persistent numbness of both upper extremities remained even after surgery; therefore, an anterior procedure or posterior decompression with corrective fusion should have been applied in this case.

DISCUSSION

LAMP has been reported to be effective, relatively low cost, minimally invasive, and safe for the treatment of patients with multilevel spondylosis or ossification of the posterior longitudinal ligament.[5–8,24] However, undesirable outcomes after LAMP can be caused by residual anterior compression of the spinal cord resulting from preoperative cervical misalignment and progression of kyphosis or loss of lordosis. The resulting pathology often reduces the quality of life and may require secondary surgery. Therefore, it is necessary to determine the factors that limit the efficacy of posterior decompression. In the current study, we optimized new indices, INT_{sum} and INT_{min}, on the basis of the mK-line and evaluated whether they could be useful for surgical treatment decisions.

We found that the interval between the mK-line and the anterior feature of the spinal column, that is, INT_n on preoperative MRI, was closely associated with the actual posterior cord shift at each vertebral level after LAMP. Furthermore, we showed that both INT_{sum} and INT_{min} were significantly higher in the lordotic group than in the nonlordotic group. These findings are consistent with the frequent observation of anterior clearance of the spinal cord in patients with a lack of cervical lordosis, thereby suggesting that the mK-line may be useful to evaluate impingement of the spinal cord by the anterior feature of the spinal column.

Furthermore, we quantified the posterior shift of the whole spinal cord as INT_{sum} for prediction of postoperative clinical outcome. Baba *et al*[23] previously showed that the magnitude of posterior cord migration after LAMP was significantly correlated with postoperative neurological outcome. In the current study, the anticipated cord migration, defined as INT_{sum}, was not associated with the RR of the JOA score. However, because patients with INT_{sum} of 20 mm or greater tended to achieve better outcomes than patients with INT_{sum} of less than 20 mm, INT_{sum} may be useful for prediction of clinical and radiological outcomes.

We also investigated the relationship between the segment responsible for the myelopathy and the level at which INT_{min} was measured. Indeed, the level at which INT_{min} was observed did not always correspond to the segment responsible for the

TABLE 3. Demographic Data for Each Group*

	Lordotic Group (n = 38)	Nonlordotic Group (n = 23)	*P*
Age, yr	67.8 ± 9.0	67.7 ± 11.0	ND
Male (%)	65.8%	82.6%	ND
Duration of symptoms, mo	11.8 ± 12.5	13.9 ± 10.9	ND
Preoperative JOA score	8.2 ± 3.2	8.5 ± 3.3	ND
Postoperative JOA score	12.5 ± 3.5	12.0 ± 2.9	ND
Recovery rate of the JOA score	51.6 ± 26.6	42.2 ± 27.4	ND
Preoperative C2–C7 lordotic angle (degrees)	25.1 ± 12.1	5.2 ± 8.0	<0.01
INT_{sum}	31.5± 7.1	20.8 ± 8.1	<0.01
INT_{min}	6.27 ± 1.9	3.38 ± 2.1	<0.01
Posterior shift of the whole spinal cord (C_{sum})	113.3 ± 95.8	77.2 ± 56.6	ND
Positive ratio of signal intensity change in the spinal cord (%)	94.7	82.6	ND
Segment responsible (cases)			
C3–C4	10	5	ND
C4–C5	12	8	ND
C5–C6	16	9	ND
C6–C7	0	1	ND
Incidence of C5 palsy	2 cases/5.3%	2 cases/8.7%	ND

**Data are expressed as the mean ± SD.*

ND indicates no significant difference; JOA, The Japanese Orthopaedic Association; INT_{sum}, sum of the intervals between the K-line and the anterior element of the spinal canal at each segment (C3–C6); INT_{min}, the minimum interval between the preoperative modified K-line and the anterior impingement on midsagittal imaging; C_n, $(B_n - A_n) \times 100/A_n$ (n = 3–6; A_n and B_n, represent the preoperative and postoperative intervals between the midpoint of the spinal cord and the anterior impingement at each segment from C3 to C6 levels); C_{sum}, sum of C3, C4, C5, and C6.

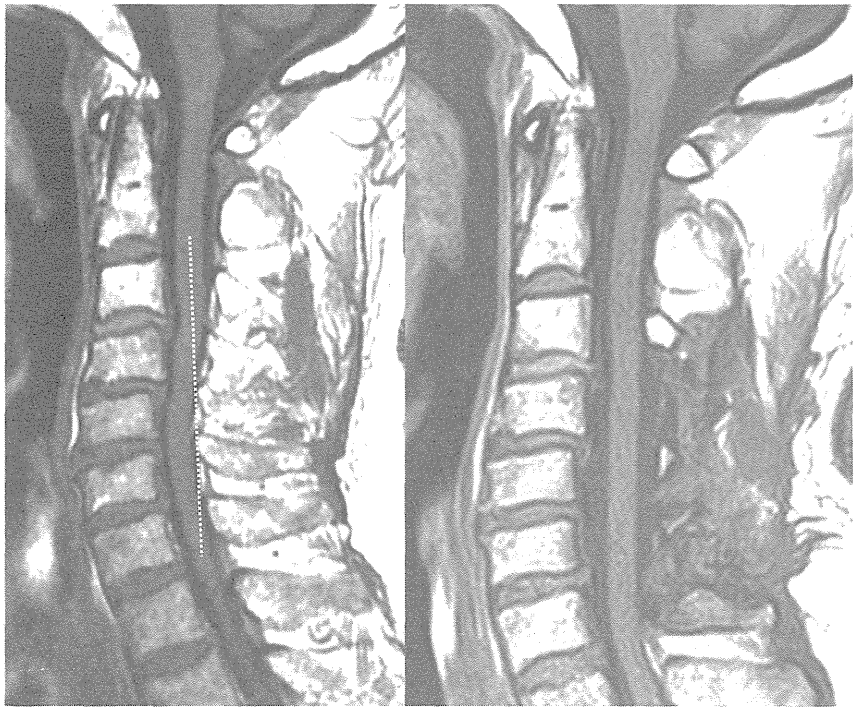

Figure 4. Preoperative magnetic resonance imaging shows that anterior compression at the C3–C4 level is caused by local kyphosis on sigmoid alignment. In this case, INT_{sum} and INT_{min} were 22.2 mm and 1.7 mm, respectively (*left*). Postoperative magnetic resonance imaging demonstrates that anterior compression of the dural sac and anterior spinal cord remained at the C3–C4 level even after posterior decompression (*right*).

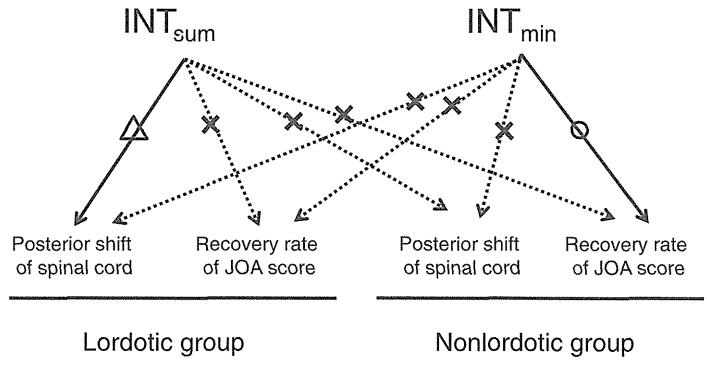

Figure 5. Summary of this study. Although INT_{sum} was associated with the magnitude of posterior cord shifting after laminoplasty in patients with lordotic alignment, it was not a predictive factor for postoperative clinical outcome. In contrast, INT_{min} was significantly correlated with postoperative neurological improvement in patients with nonlordotic alignment, whereas there was no association between INT_{min} and the degree of posterior cord shifting. JOA indicates The Japanese Orthopaedic Association.

myelopathy diagnosed by electrophysiology; in 10 patients, the segment responsible for myelopathy was typically C4–C5 or C5–C6, whereas the level with the highest compression was C3–C4 or C6–C7. Two of these 10 patients could not obtain sufficient cord migration at the C3–C4 level and thus obtained unsatisfactory outcomes. In such cases, it is still important to pay attention to the level with the highest compression, although it is not diagnosed as the causative segment by electrophysiologic and neurological findings, because residual cord compression in the noncausative segment still contributes to the myelopathic symptomatology and is thus a risk factor for myelopathic deterioration after LAMP.

In addition, we also investigated whether the anticipated cord migration could predict the onset of C5 palsy, which is a major complication after LAMP[25] and for which excessive posterior cord shift has been considered as a possible cause. However, we did not observe a significant association between the degree of posterior cord shifting and the incidence of C5 palsy. Previous reports have suggested various other causes for C5 palsy after LAMP, including (1) nerve root traction caused by posterior spinal cord shifting,[26] (2) anatomical stenosis of the C5 foramen,[27] (3) spinal cord ischemia caused by decreased blood supply from radicular arteries,[28] (4) laminar width of decompression,[29] and (5) segmental spinal cord disorder.[25,30] These factors may contribute to the onset of postoperative C5 palsy in a complex manner, and it may, therefore, not be possible to predict the C5 palsy by only measuring the anticipated cord shift.

The relationship between cervical kyphotic alignment and postoperative clinical outcomes after LAMP is controversial. Suda *et al*[13] reported that LAMP is not effective for patients with global kyphosis greater than 13° and no signal change on T2-weighted MR image. Uchida *et al*[31] suggested that correction of local sagittal alignment should be attempted in patients with kyphotic deformity greater than 10° to maximize neurological improvement. Thus, because excessive kyphotic alignment has been recognized as a risk factor for poor outcomes after posterior decompression over the last decade, many studies have recommended that anterior decompression or posterior decompression with fusion should be applied to such misalignment cases.[5,13,31]

However, Kaptain *et al*[32] investigated 46 patients with CSM and concluded that clinical outcome does not usually correlate with preoperative sagittal alignment. This report is consistent with mounting evidence that neurological improvement is influenced by not only global kyphosis but also anterior compression of the spinal cord, which seems to lead to a lack of decompression at the ventral aspect of the spinal cord.[5,11,13,23] Given these 2 morphological factors, it is important to evaluate the physical relationship between the spinal cord and the anterior impingement that may be causing the compression prior to surgical treatment. In addition, spine surgeons should predict postoperative clinical outcomes before selecting a surgical procedure for the treatment of CSM particularly in patients with cervical misalignment. This study demonstrated that neurological improvement after LAMP in patients with nonlordotic alignment was significantly correlated with INT_{min} but not with INT_{sum} (Figure 5). Therefore, neurological improvement in patients with misalignment may require a sufficient posterior cord shift at only the most compressed segment rather than throughout the entire spinal cord.

The limitations of this study include its retrospective nature and relatively small cohort size. In the present study, we divided the patients into only 2 groups and showed that INT_{min} significantly predicted postoperative outcome; however, it may be possible to categorize a larger patient pool into 5 different alignments to determine the relationship between our new index and clinical outcomes in each alignment type. With regard to neck position, although our patients were instructed to maintain a neutral position, this was not usually possible during MRI; however, because all patients followed the same radiographical protocol and alignment on MRI was significantly correlated with alignment measured by neutral radiography, the lack of neutral position does not affect the findings of this study. We, therefore, suggest that INT_{min} can help spine surgeons to decide whether LAMP should be performed in patients with nonlordotic alignment.

➢ Key Points

- ❑ Patients who underwent LAMP for the treatment of CSM were divided into lordosis and nonlordosis groups, and we investigated whether anterior clearance of the spinal cord measured on mK-line plays role for predictive factors of postoperative spinal cord migration and clinical outcome in this study.

- Anterior clearance of global spinal cord (INT_{sum}) tends to be associated with the posterior shift of the spinal cord in patients with lordotic alignment but not in patients with nonlordotic alignment.
- INT_{sum} was not associated with clinical outcome in either lordosis group or nonlordosis group.
- A linear regression analysis showed that anticipated anterior clearance at the most compressive segment (INT_{min}) was a significant predictive factor for postoperative clinical outcome in patients with nonlordotic alignment.

Acknowledgments

Drs. Takashi Taniyama and Takashi Hirai contributed equally to this work.

References

1. Hirabayashi K, Watanabe K, Wakano K, et al. Expansive open-door laminoplasty for cervical spinal stenotic myelopathy. *Spine (Phila Pa 1976)* 1983;8:693–9.
2. Kawai S, Sunago K, Doi K, et al. Cervical laminoplasty (Hattori's method). Procedure and follow-up results. *Spine (Phila Pa 1976)* 1988;13:1245–50.
3. Tsuji H. Laminoplasty for patients with compressive myelopathy due to so-called spinal canal stenosis in cervical and thoracic regions. *Spine (Phila Pa 1976)* 1982;7:28–34.
4. Oyama M, Hattori S. A new method of posterior decompression [in Japanese]. *Central Jpn J Orthop Traumatic Surg.* 1973;16:792–4.
5. Hirai T, Okawa A, Arai Y, et al. Middle-term results of a prospective comparative study of anterior decompression with fusion and posterior decompression with laminoplasty for the treatment of cervical spondylotic myelopathy. *Spine (Phila Pa 1976)* 2011;36:1940–7.
6. Subramaniam V, Chamberlain RH, Theodore N, et al. Biomechanical effects of laminoplasty versus laminectomy: stenosis and stability. *Spine (Phila Pa 1976)* 2009;34:E573–8.
7. Seichi A, Takeshita K, Ohishi I, et al. Long-term results of double-door laminoplasty for cervical stenotic myelopathy. *Spine (Phila Pa 1976)* 2001;26:479–87.
8. Chiba K, Ogawa Y, Ishii K, et al. Long-term results of expansive open-door laminoplasty for cervical myelopathy—average 14-year follow-up study. *Spine (Phila Pa 1976)* 2006;31:2998–3005.
9. Tani T, Ushida T, Ishida K, et al. Relative safety of anterior microsurgical decompression versus laminoplasty for cervical myelopathy with a massive ossified posterior longitudinal ligament. *Spine (Phila Pa 1976)* 2002;27:2491–8.
10. Iwasaki M, Okuda S, Miyauchi A, et al. Surgical strategy for cervical myelopathy due to ossification of the posterior longitudinal ligament. Part 1: clinical results and limitations of laminoplasty. *Spine (Phila Pa 1976)* 2007;32:647–53.
11. Hirai T, Kawabata S, Enomoto M, et al. Presence of anterior compression of the spinal cord after laminoplasty inhibits upper extremity motor recovery in patients with cervical spondylotic myelopathy. *Spine (Phila Pa 1976)* 2012;37:377–84.
12. Taniyama T, Hirai T, Yamada T, et al. Modified K-line in magnetic resonance imaging predicts insufficient decompression of cervical laminoplasty. *Spine (Phila Pa 1976)* 2013;38:496–501.
13. Suda K, Abumi K, Ito M, et al. Local kyphosis reduces surgical outcomes of expansive open-door laminoplasty for cervical spondylotic myelopathy. *Spine (Phila Pa 1976)* 2003;28:1258–62.
14. Kamata M, Hirabayashi K, Satomi K, et al. Postoperative spinal deformity by posterior decompression for cervical spondylotic myelopathy [in Japanese]. *East Jpn J Clin Orthop* 1990;2:86–9.
15. Matsumoto M, Fujimura Y, Suzuki N, et al. Cervical curvature in acute whiplash injuries: prospective comparative study with asymptomatic subjects. *Injury.* 1998;29:775–8.
16. Miyazaki K, Kirita Y. Extensive simultaneous multisegment laminectomy for myelopathy due to the ossification of the posterior longitudinal ligament in the cervical region. *Spine (Phila Pa 1976)* 1986;11:531–42.
17. The Japanese Orthopaedic Association. Criteria for the evaluation of treatment of cervical myelopathy. *J Jpn Orthop Assoc (Tokyo)* 1976;49:Addenda No 12.
18. Hirabayashi K, Miyakawa J, Satomi K, et al. Operative results and postoperative progression of ossification among patients with ossification of cervical posterior longitudinal ligament. *Spine (Phila Pa 1976)* 1981;6:354–64.
19. Fujiyoshi T, Yamazaki M, Kawabe J, et al. A new concept for making decisions regarding the surgical approach for cervical ossification of the posterior longitudinal ligament: the K-line. *Spine (Phila Pa 1976)* 2008;33:E990–3.
20. Yamazaki A, Homma T, Uchiyama S, et al. Morphologic limitations of posterior decompression by midsagittal splitting method for myelopathy caused by ossification of the posterior longitudinal ligament in the cervical spine. *Spine (Phila Pa 1976)* 1999;24:32–4.
21. Yonenobu K, Okada K, Fuji T, et al. Causes of neurologic deterioration following surgical treatment of cervical myelopathy. *Spine (Phila Pa 1976)* 1986;11:818–23.
22. Morio Y, Yamamoto K, Kuranobu K, et al. Does increased signal intensity of the spinal cord on MR images due to cervical myelopathy predict prognosis? *Arch Orthop Trauma Surg* 1994;113:254–9.
23. Baba H, Uchida K, Maezawa Y, et al. Lordotic alignment and posterior migration of the spinal cord following en bloc open-door laminoplasty for cervical myelopathy: a magnetic resonance imaging study. *J Neurol* 1996;243:626–32.
24. Sakai K, Okawa A, Takahashi M, et al. Five-year follow-up evaluation of surgical treatment for cervical myelopathy caused by ossification of the posterior longitudinal ligament: a prospective comparative study of anterior decompression and fusion with floating method versus laminoplasty. *Spine (Phila Pa 1976)* 2012;37:367–76.
25. Sakaura H, Hosono N, Mukai Y, et al. C5 palsy after decompression surgery for cervical myelopathy: review of the literature. *Spine (Phila Pa 1976)* 2003;28:2447–51.
26. Satomi K, Nishu Y, Kohno T, et al. Long-term follow-up studies of open-door expansive laminoplasty for cervical stenotic myelopathy. *Spine (Phila Pa 1976)* 1994;19:507–10.
27. Shinomiya K, Okawa A, Nakao K, et al. Morphology of C5 ventral nerve rootlets as part of dissociated motor loss of deltoid muscle. *Spine (Phila Pa 1976)* 1994;19:2501–4.
28. Komagata M, Nishiyama M, EndohK, et al. Clinical study of the postoperative C5 palsy after cervical expansive laminoplasty; efficacy of bilateral partial foraminotomy for the prevention the C5 palsy [in Japanese]. *J Jpn Spine Res Soc* 2002;131:237.
29. Lubelski D, Derakhshan A, Nowacki AS, et al. Predicting C5 palsy via the use of preoperative anatomic measurements. *Spine J* 2014;14:1895–901.
30. Ohkubo H, Komori H, Ohkawa A, et al. An investigation of the postoperative C5 palsy [in Japanese]. *J Jpn Spine Res Soc* 2002;13:354.
31. Uchida K, Nakajima H, Sato R, et al. Cervical spondylotic myelopathy associated with kyphosis or sagittal sigmoid alignment: outcome after anterior or posterior decompression. *J Neurosurg Spine* 2009;11:521–8.
32. Kaptain GJ, Simmons NE, Replogle RE, et al. Incidence and outcome of kyphotic deformity following laminectomy for cervical spondylotic myelopathy. *J Neurosurg* 2000;93:199–204.

nature genetics

A genome-wide association study identifies susceptibility loci for ossification of the posterior longitudinal ligament of the spine

Masahiro Nakajima[1,30], Atsushi Takahashi[2,30], Takashi Tsuji[3,29], Tatsuki Karasugi[1,4], Hisatoshi Baba[5], Kenzo Uchida[5], Shigenori Kawabata[6], Atsushi Okawa[6], Shigeo Shindo[7], Kazuhiro Takeuchi[8], Yuki Taniguchi[9], Shingo Maeda[10], Masafumi Kashii[11], Atsushi Seichi[12], Hideaki Nakajima[5], Yoshiharu Kawaguchi[13], Shunsuke Fujibayashi[14], Masahiko Takahata[15], Toshihiro Tanaka[16], Kei Watanabe[17], Kazunobu Kida[18], Tsukasa Kanchiku[19], Zenya Ito[20], Kanji Mori[21], Takashi Kaito[22], Sho Kobayashi[23], Kei Yamada[24], Masahito Takahashi[25], Kazuhiro Chiba[3,29], Morio Matsumoto[3], Ken-Ichi Furukawa[26], Michiaki Kubo[27], Yoshiaki Toyama[3], Genetic Study Group of Investigation Committee on Ossification of the Spinal Ligaments[28] & Shiro Ikegawa[1]

Ossification of the posterior longitudinal ligament of the spine (OPLL) is a common spinal disorder among the elderly that causes myelopathy and radiculopathy. To identify genetic factors for OPLL, we performed a genome-wide association study (GWAS) in ~8,000 individuals followed by a replication study using an additional ~7,000 individuals. We identified six susceptibility loci for OPLL: 20p12.3 (rs2423294: $P = 1.10 \times 10^{-13}$), 8q23.1 (rs374810: $P = 1.88 \times 10^{-13}$), 12p11.22 (rs1979679: $P = 4.34 \times 10^{-12}$), 12p12.2 (rs11045000: $P = 2.95 \times 10^{-11}$), 8q23.3 (rs13279799: $P = 1.28 \times 10^{-10}$) and 6p21.1 (rs927485: $P = 9.40 \times 10^{-9}$). Analyses of gene expression in and around the loci suggested that several genes are involved in OPLL etiology through membranous and/or endochondral ossification processes. Our results bring new insight to the etiology of OPLL.

OPLL (MIM 602475) is a common disease caused by abnormal ossification of the posterior longitudinal ligament in the spinal canal, affecting 0.8–3.0% of Asians and 0.1–1.7% of European Caucasians[1]. The ossified ligament compresses the spinal cord and nerve root, causing serious neurological dysfunction[2]. Several lines of evidence suggest that genetic factors contribute to its etiology and pathogenesis[3–5]; affected sibling-pair linkage studies and candidate gene association studies have identified a number of genes or loci that are linked to OPLL susceptibility[6–8]. However, replication studies have failed to verify these results, even in the same ancestry groups as the original studies[9]. A GWAS using high-density SNP data has not yet been reported for OPLL.

To identify OPLL susceptibility genes, we conducted a GWAS in a Japanese population consisting of 1,130 individuals with OPLL and 7,135 controls (Online Methods). After quality control filtering of SNP genotyping data (Online Methods), 616,496 autosomal SNPs were examined for association with the Cochran-Armitage trend test. Analysis of population stratification with principal-component analysis (PCA) showed that all individuals in our study were Japanese

[1]Laboratory for Bone and Joint Diseases, Center for Integrative Medical Sciences, RIKEN, Tokyo, Japan. [2]Laboratory for Statistical Analysis, Center for Integrative Medical Sciences, RIKEN, Yokohama, Japan. [3]Department of Orthopaedic Surgery, School of Medicine, Keio University, Tokyo, Japan. [4]Department of Orthopaedic and Neuro-Musculoskeletal Surgery, Faculty of Medical and Pharmaceutical Sciences, Kumamoto University, Kumamoto, Japan. [5]Department of Orthopaedics and Rehabilitation Medicine, Faculty of Medical Sciences, University of Fukui, Fukui, Japan. [6]Department of Orthopaedic Surgery, Tokyo Medical and Dental University, Tokyo, Japan. [7]Department of Orthopedics, Kudanzaka Hospital, Tokyo, Japan. [8]Department of Orthopaedic Surgery, National Okayama Medical Center, Okayama, Japan. [9]Department of Orthopaedic Surgery, Faculty of Medicine, The University of Tokyo, Tokyo, Japan. [10]Department of Medical Joint Materials, Graduate School of Medical and Dental Sciences, Kagoshima University, Kagoshima, Japan. [11]Department of Orthopaedic Surgery, Osaka University Graduate School of Medicine, Osaka, Japan. [12]Department of Orthopedics, Jichi Medical University, Shimotsuke, Japan. [13]Department of Orthopaedic Surgery, Toyama University, Toyama, Japan. [14]Department of Orthopaedic Surgery, Graduate School of Medicine, Kyoto University, Kyoto, Japan. [15]Department of Orthopedic Surgery, Hokkaido University Graduate School of Medicine, Sapporo, Japan. [16]Department of Orthopaedic Surgery, Hirosaki University Graduate School of Medicine, Hirosaki, Japan. [17]Department of Orthopaedic Surgery, Niigata University Medical and Dental General Hospital, Niigata, Japan. [18]Department of Orthopaedic Surgery, Kochi Medical School, Kochi, Japan. [19]Department of Orthopedic Surgery, Yamaguchi University Graduate School of Medicine, Ube, Japan. [20]Department of Orthopedics, Nagoya University Graduate School of Medicine, Nagoya, Japan. [21]Department of Orthopaedic Surgery, Shiga University of Medical Science, Otsu, Japan. [22]Department of Orthopaedic Surgery, National Hospital Organization Osaka Minami Medical Center, Osaka, Japan. [23]Department of Orthopaedic Surgery, Hamamatsu University School of Medicine, Hamamatsu, Japan. [24]Department of Orthopaedic Surgery, Kurume University School of Medicine, Kurume, Japan. [25]Department of Orthopaedic Surgery, Kyorin University School of Medicine, Tokyo, Japan. [26]Department of Pharmacology, Hirosaki University Graduate School of Medicine, Hirosaki, Japan. [27]Laboratory for Genotyping Development, Center for Integrative Medical Sciences, RIKEN, Yokohama, Japan. [28]A full list of members and affiliations appears in the **Supplementary Note**. [29]Present address: Department of Orthopaedic Surgery, Kitasato University Kitasato Institute Hospital, Tokyo, Japan. [30]These authors contributed equally to this work. Correspondence should be addressed to S.I. (sikegawa@ims.u-tokyo.ac.jp).

Received 20 February; accepted 30 June; published online 27 July 2014; doi:10.1038/ng.3045

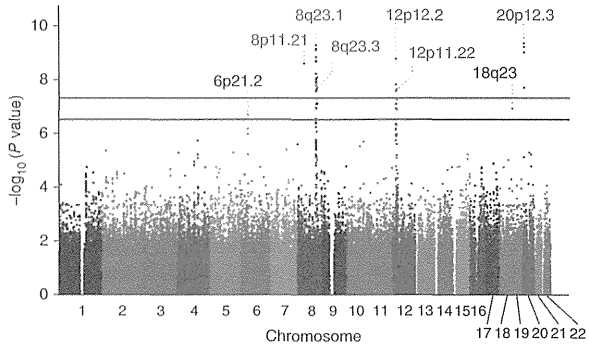

Figure 1 Manhattan plot showing the $-\log_{10}$ *P* value for each SNP in the GWAS. Values were plotted against their respective positions on the autosomal chromosomes. The red line represents the genome-wide significance threshold ($P = 5 \times 10^{-8}$). The blue line represents the threshold for the selection of SNPs for the replication study ($P = 5 \times 10^{-7}$).

(**Supplementary Fig. 1a**); however, there was a small proportion of samples that were separated from the major Japanese (Hondo) cluster[10] when PCA was performed using only the genotype information for the cases and controls in the study (**Supplementary Fig. 1b**). We used samples from the major Japanese cluster consisting of 1,112 cases and 6,810 controls (**Supplementary Table 1**) and generated a quantile-quantile plot (**Supplementary Fig. 1c**). We found that the genomic inflation factor (λ_{GC}) was 1.01, indicating that there was a low possibility of false positive associations resulting from population stratification. Twenty-six SNPs within six chromosomal regions at 8p11.21, 8q23.1, 8q23.3, 12p12.2, 12p11.22 and 20p12.3 had associations that reached the genome-wide significance threshold of $P < 5 \times 10^{-8}$ (**Fig. 1** and **Supplementary Table 2**). We further found an additional two loci (6p21.2 and 18q23) showing suggestive association with OPLL ($P < 5 \times 10^{-7}$; **Fig. 1** and **Supplementary Table 2**). To investigate additional susceptibility loci, we obtained whole-genome association results for imputed SNPs. We found that 895 SNPs in the 8 identified loci were associated at $P < 5 \times 10^{-7}$, and no other associated loci were uncovered. We also examined 12,228 SNPs on the X chromosome for association with OPLL and found no significant association.

To confirm the associations at the eight loci, we selected the eight SNPs that had the smallest *P* value at each locus for the replication study. We genotyped an independent set of 548 Japanese individuals with OPLL and 6,469 Japanese controls (**Supplementary Table 1**), finding significant associations for 5 of the 8 SNPs, even after Bonferroni correction with $P < 6.25 \times 10^{-3}$ (0.05/8) (**Table 1** and **Supplementary Table 2**). Combining the results from the GWAS and replication study, six SNPs reached a genome-wide significance threshold of $P < 9.68 \times 10^{-9}$ (0.05/5,163,786) (**Table 1** and **Supplementary Table 3**). The Breslow-Day test for these six SNPs showed an absence of significant heterogeneity ($P > 0.05$) between studies. We carried out age- and sex-adjusted analyses using a logistic regression model and confirmed similar association after adjustment (**Supplementary Table 4**). We next conducted conditional analysis to adjust for the top SNPs at these six loci using the GWAS data. There were no independently associated signals in the six loci (**Supplementary Fig. 2**).

The most highly associated SNP in the meta-analysis, rs2423294 ($P_{combined} = 1.10 \times 10^{-13}$), was located in the 3′ flanking region of *HAO1* at 20p12.3 (**Fig. 2a**). *HAO1* is expressed primarily in the liver and pancreas and encodes hydroxyacid oxidase, which oxidizes 2-hydroxyacid. We identified 80 imputed SNPs in this region that reached a genome-wide significance threshold for association ($P < 5 \times 10^{-8}$); 71 highly associated SNPs ($P < 1 \times 10^{-9}$) were located in the 3′ flanking region of *HAO1* (**Fig. 2a**).

The associated region at 8q23.1 contained three genes—*RSPO2*, *EIF3E* and *EMC2* (**Fig. 2b**). *RSPO2* encodes a member of the R-spondin family of secreted proteins that are involved in β-catenin activation through canonical Wnt/β-catenin signaling[11], which is indispensable for osteoblastogenesis[12]. Reduced expression of R-spondin 2 has been reported in osteoarthritis-derived osteoblasts, and Wnt-dependent mineralization of osteoblasts is promoted by R-spondin 2 (ref. 13). *EIF3E* encodes a component of the eukaryotic translation initiation factor 3 (eIF-3) complex, which is required for several steps in the initiation of protein synthesis. The eIF-3 complex

Table 1 Association of the six genome-wide significant loci

SNP ID	Allele (risk allele)	Chromosome	Genes in or near associated region[a]	Study	RAF Case	RAF Control	*P* value[b]	OR (95% CI)[c]	P_{het}[d]
rs2423294	T/C (T)	20p12.3	***HAO1***	GWAS	0.207	0.155	4.90×10^{-10}	1.43 (1.27–1.60)	
				Replication	0.203	0.155	4.00×10^{-5}	1.38 (1.19–1.62)	
				Combined[e]	0.205	0.155	1.10×10^{-13}	1.41 (1.29–1.55)	0.757
rs374810	A/G (G)	8q23.1	***RSPO2, EIF3E, EMC2***	GWAS	0.676	0.607	5.79×10^{-10}	1.35 (1.23–1.49)	
				Replication	0.675	0.615	8.88×10^{-5}	1.30 (1.14–1.49)	
				Combined[e]	0.676	0.611	1.88×10^{-13}	1.34 (1.24–1.44)	0.651
rs1979679	T/C (T)	12p11.22	***CCDC91***	GWAS	0.422	0.360	2.42×10^{-8}	1.30 (1.18–1.42)	
				Replication	0.426	0.364	4.75×10^{-5}	1.30 (1.14–1.47)	
				Combined[e]	0.423	0.362	4.34×10^{-12}	1.30 (1.21–1.40)	0.994
rs11045000	A/G (A)	12p12.2	***LOC100506393***	GWAS	0.523	0.454	1.74×10^{-9}	1.32 (1.20–1.44)	
				Replication	0.514	0.466	2.35×10^{-3}	1.21 (1.07–1.37)	
				Combined[e]	0.520	0.460	2.95×10^{-11}	1.28 (1.19–1.38)	0.281
rs13279799	A/G (G)	8q23.3	*LINC00536, EIF3H*	GWAS	0.378	0.317	8.96×10^{-9}	1.31 (1.19–1.44)	
				Replication	0.368	0.322	1.80×10^{-3}	1.23 (1.08–1.39)	
				Combined[e]	0.375	0.319	1.28×10^{-10}	1.28 (1.19–1.38)	0.416
rs927485	T/C (C)	6p21.1	*CDC5L, MIR4642, SUPT3H*	GWAS	0.176	0.134	2.10×10^{-7}	1.37 (1.22–1.55)	
				Replication	0.169	0.140	8.19×10^{-3}	1.25 (1.06–1.48)	
				Combined[e]	0.173	0.137	9.40×10^{-9}	1.33 (1.21–1.46)	0.372

RAF, risk allele frequency; OR, odds ratio; CI, confidence interval.
[a]Genes in the LD block of the associated SNPs are shown in bold. [b]Results from the Cochran-Armitage trend test. [c]Estimated for the risk allele from a 2 × 2 allele frequency table. [d]Results from the Breslow-Day test. [e]Calculated by the Mantel-Haenszel method.

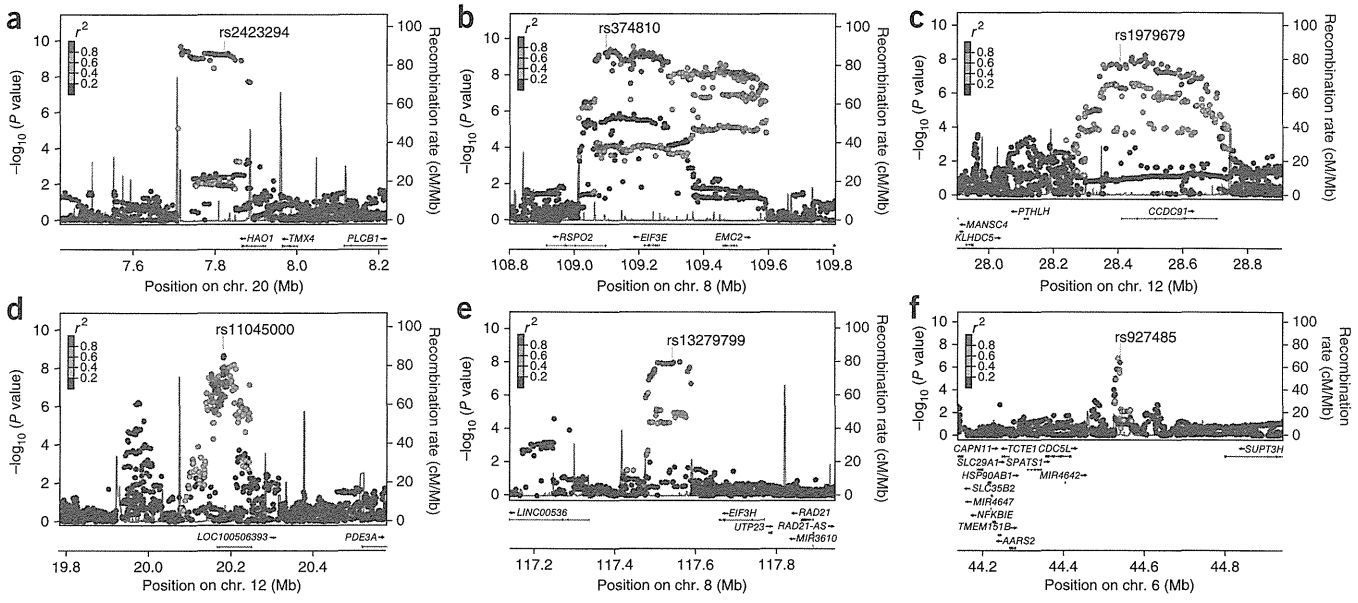

Figure 2 Regional association plots at six susceptibility loci for OPLL. Each plot shows $-\log_{10}$ *P* values against the chromosomal positions of SNPs in the specific region. The genotyped SNP with the strongest association signal in each locus is represented as a purple diamond; the other SNPs are colored according to the extent of LD with this SNP. Estimated recombination rates from the hg19/1000 Genomes Project March 2012 East Asian reference are shown as light-blue lines. (**a**) 20p12.3. (**b**) 8q23.1. (**c**) 12p11.22. (**d**) 12p12.2. (**e**) 8q23.3. (**f**) 6p21.1.

stimulates mRNA recruitment to the 43S preinitiation complex and scanning of the mRNA for recognition of the translation initiation codon[14]. *EMC2* encodes a component of the endoplasmic reticulum membrane protein complex[15]; however, its cellular function is unclear.

The chromosome 12p11.22 region contained *CCDC91* (**Fig. 2c**), which encodes a protein involved in the trans-Golgi network. Notably, the associated region was located adjacent to the *PTHLH* gene, which encodes a member of the parathyroid hormone (PTH) family. PTH, via its receptor PTH1R, regulates endochondral ossification, which is related to OPLL progression[16]. Associated SNPs at the 12p12.2 locus were in *LOC100506393* (**Fig. 2d**), which is predicted to encode a large intergenic noncoding RNA (lincRNA). *LOC100506393* consists of three exons and has no similarity to known orthologous transcripts. The associated region at 8q23.3 was located in a gene desert between *LINC00536* and *EIF3H* (**Fig. 2e**). *LINC00536* encodes a lincRNA of unknown function. *EIF3H* encodes a component of the eIF-3 complex, as does *EIF3E*. The fact that two of the six loci for OPLL harbor genes encoding proteins in the eIF-3 complex suggests that aberrations in this pathway might be key in OPLL pathogenesis.

The associated region at 6p21.1 was located in the gene desert between *CDC5L*, *MIR4642* and *SUPT3H* (**Fig. 2f**). The cell division cycle 5–like protein encoded by the *CDC5L* gene is a positive regulator of G2/M progression in the cell cycle[17]. CDC5L was also found to be a core component of a putative E3 ubiquitin ligase complex. This complex has been shown to have a role in pre-mRNA splicing from yeast to humans[18]. *MIR4642*, located in intron 14 of the *CDC5L* gene, encodes a microRNA whose target genes and functions are unknown. *SUPT3H* encodes a human homolog of Spt3, which is a *Saccharomyces cerevisiae* transcription factor required for the transcription of a number of RNA polymerase II–transcribed genes[19]. An association of bone mineral density in the lumbar spine with a SNP (rs11755164) 155 kb downstream of the *SUPT3H* gene has been reported[20], but this SNP was not in linkage disequilibrium (LD) with rs927485 ($D' = 0.013$, $r^2 = 0$).

Fifteen genes or loci have previously been reported to be associated with OPLL. We investigated the GWAS data for these reported genes but found no significant association (**Supplementary Table 5**). A genome-wide linkage study reported five loci that showed suggestive linkage after stratification by OPLL severity, age at diagnosis and associated diabetes mellitus[21]. One of the six SNPs that showed genome-wide significant association with OPLL, rs2423294 ($P_{combined} = 1.10 \times 10^{-13}$), was located in the linkage region at 20p12.3 (**Supplementary Fig. 3**). We stratified the cases from our GWAS according to the previous linkage study[21] and investigated the associations of the SNPs in the linkage regions. In all strata, the OR estimates for association increased after stratification (**Supplementary Table 6**). A stratum of subjects without diabetes mellitus showed genome-wide significant association at rs10486860 in the 7q22 linkage region ($P = 4.31 \times 10^{-8}$), suggesting that OPLL is genetically heterogeneous and that the locus is associated with a subtype of OPLL. Association of diabetes mellitus in individuals with OPLL and the contribution of abnormal insulin metabolism to OPLL have been reported[22].

To understand the functional roles of the loci and genes associated with OPLL, we first examined expression of the candidate genes within the LD blocks for the associated SNPs (**Fig. 2**). We assessed the mRNA expression of these six genes in human bone cells and fibroblasts by RT-PCR. *EIF3E*, *EMC2* and *CCDC91* were abundantly expressed in both cells, whereas *HAO1*, *RSPO2* and *LOC100506393* expression was absent in these cells (**Supplementary Fig. 4**). There was no difference in the expression of the genes in the two cell types. We then examined the expression of these genes in the ATDC5 cell line, a mouse model of endochondral ossification[23]. Expression of *Hoa1*, *Rspo2* and *Ccdc91* was lower during early stages of chondrogenesis, whereas expression of *Sox9*, the master gene for chondrogenesis, was higher; in later stages, the expression of cartilage matrix genes (*Acan* and *Col2a1*) was increased (**Supplementary Fig. 5**).

We next investigated the 63 genes within 1 Mb of the associated SNPs for differential expression in osteoblasts and fibroblasts. We examined the cell type–specific gene expression profile using the

FANTOM5 SSTAR database[24]. The expression of four genes was increased by >2-fold in osteoblasts, whereas the expression of six genes was increased by >2-fold in fibroblasts (**Supplementary Table 7**). We examined the ten genes that showed differential expression in quantitative PCR (qPCR) experiments and confirmed increased gene expression of *RSPH9* and *STK38L* in osteoblasts (**Supplementary Table 7**), suggesting that these genes have a role in membranous ossification. The protein encoded by the *RSPH9* gene is a component of the radial spoke head in motile cilia and flagella[25]. The primary cilia machinery has a critical role in the Hedgehog signaling pathway in skeletal development and has been implicated in a dozen disorders known as skeletal ciliopathies[26]. *STK38L* encodes a serine/threonine protein kinase that controls the protein stability of the cyclin-dependent kinase inhibitor protein p21 through direct phosphorylation and inhibits G1/S progression through the cell cycle[27]. We further investigated expression of the 63 genes in mesenchymal stem cells (MSCs) from the spinal ligament. We compared gene expression between the MSCs obtained from subjects with and without OPLL[28] using a cDNA microarray and confirmed differential expression by qPCR. There was no significant difference in the expression of the genes within 1 Mb of the associated SNPs (data not shown).

To gain additional information regarding the function of the SNPs, we examined all publically available expression quantitative trait locus (eQTL) data (Genevar) obtained from the analysis of a lymphoblastoid cell line[29]. There was no evidence of a significant association between genotype and gene expression ($P > 0.05$ after adjustment for multiple testing). We applied literature-based pathway analysis, using GRAIL[30] to investigate the connections between genes in the OPLL-associated loci. We used 6 regions that had a significant genome-wide association as query regions, resulting in the analysis of 12 unique genes. We found a subset of two SNPs with a functional connection (GRAIL $P < 0.05$)—*EIF3E* (rs374810; $P = 0.020$) and *EIF3H* (rs13279799; $P = 0.021$)—with members of the translation initiation pathway.

In summary, through a GWAS and replication study in Japanese populations, we identified six new susceptibility loci for OPLL. One of these overlapped with a previously reported linkage region. Analyses of gene expression in and around the OPLL-associated loci suggested that *RSPH9* and *STK38L* might be involved in OPLL etiology through the membranous ossification process and that *HAO1*, *RSPO2* and *CCDC91* might be involved through the endochondral ossification process. Additional genetic and functional studies for the loci and genes identified by our study should aid in clarification of the etiology and pathogenesis of OPLL.

URLs. 1000 Genomes Project, http://www.1000genomes.org/; Genevar, http://www.sanger.ac.uk/resources/software/genevar/; GRAIL, http://www.broadinstitute.org/mpg/grail/; FANTOM5 SSTAR, http://fantom.gsc.riken.jp/5/sstar/Main_Page; EIGENSTRAT, http://genetics.med.harvard.edu/reich/Reich_Lab/Software.html; Minimac, http://genome.sph.umich.edu/wiki/Minimac; LocusZoom, http://csg.sph.umich.edu/locuszoom/; PLINK, http://pngu.mgh.harvard.edu/~purcell/plink/.

METHODS

Methods and any associated references are available in the online version of the paper.

Note: Any Supplementary Information and Source Data files are available in the online version of the paper.

ACKNOWLEDGMENTS

We thank the individuals with OPLL and their families who participated in this study and the Japan OPLL Network (Zen-Sekichu-Ren), including Ishikawa prefecture OPLL Tomo-no-kai. We also thank Y. Takahashi and T. Oguma for technical assistance. The work reported in this article was supported by grants from the Ministry of Health, Labour and Welfare of Japan: Committee for Study of Ossification of Spinal Ligament (H23-Nanchi-Ippan-032) and Committee for Research and Development of Therapies for Ossification of Posterior Longitudinal Ligament (H26-Itaku(Nan)-Ippan-053).

AUTHOR CONTRIBUTIONS

S.I. designed the project and provided overall project management. M.N. and S.I. drafted the manuscript. M.N. and M. Kubo performed the genotyping for the GWAS. A.T. analyzed the GWAS data. T. Tsuji, T. Karasugi, H.B., K.U., S. Kawabata, A.O., S.S., K.T., Y. Taniguchi, S.M., M. Kashii, A.S., H.N., Y.K., S.F., M. Takahata, T. Tanaka, K.W., K.K., T. Kanchiku, Z.I., K.M., T. Kaito, S. Kobayashi, K.Y., M. Takahashi, K.C., M.M., K.-I.F. and Y. Toyama managed the DNA samples and clinical data.

COMPETING FINANCIAL INTERESTS

The authors declare no competing financial interests.

1. Matsunaga, S. & Sakou, T. in *OPLL: Ossification of the Posterior Longitudinal Ligament* 2nd edn. (eds. Yonenobu, K., Nakamura, K. & Toyama, Y.) 11–17 (Springer, Tokyo, 2006).
2. Matsunaga, S. *et al.* Pathogenesis of myelopathy in patients with ossification of the posterior longitudinal ligament. *J. Neurosurg.* **96**, 168–172 (2002).
3. Sakou, T., Matsunaga, S. & Koga, H. Recent progress in the study of pathogenesis of ossification of the posterior longitudinal ligament. *J. Orthop. Sci.* **5**, 310–315 (2000).
4. Taketomi, E., Sakou, T., Matsunaga, S. & Yamaguchi, M. Family study of a twin with ossification of the posterior longitudinal ligament in the cervical spine. *Spine* **17**, S55–S56 (1992).
5. Okawa, A. *et al.* Mutation in *Npps* in a mouse model of ossification of the posterior longitudinal ligament of the spine. *Nat. Genet.* **19**, 271–273 (1998).
6. Koga, H. *et al.* Restriction fragment length polymorphism of genes of the α2(XI) collagen, bone morphogenetic protein-2, alkaline phosphatase, and tumor necrosis factor-α among patients with ossification of posterior longitudinal ligament and controls from the Japanese population. *Spine* **21**, 469–473 (1996).
7. Nakamura, I. *et al.* Association of the human *NPPS* gene with ossification of the posterior longitudinal ligament of the spine (OPLL). *Hum. Genet.* **104**, 492–497 (1999).
8. Tanaka, T. *et al.* Genomewide linkage and linkage disequilibrium analyses identify *COL6A1*, on chromosome 21, as the locus for ossification of the posterior longitudinal ligament of the spine. *Am. J. Hum. Genet.* **73**, 812–822 (2003).
9. Horikoshi, T. *et al.* A large-scale genetic association study of ossification of the posterior longitudinal ligament of the spine. *Hum. Genet.* **119**, 611–616 (2006).
10. Yamaguchi-Kabata, Y. *et al.* Japanese population structure, based on SNP genotypes from 7003 individuals compared to other ethnic groups: effects on population-based association studies. *Am. J. Hum. Genet.* **83**, 445–456 (2008).
11. Kim, K.A. *et al.* R-spondin proteins: a novel link to β-catenin activation. *Cell Cycle* **5**, 23–26 (2006).
12. Monroe, D.G., McGee-Lawrence, M.E., Oursler, M.J. & Westendorf, J.J. Update on Wnt signaling in bone cell biology and bone disease. *Gene* **492**, 1–18 (2012).
13. Abed, É. *et al.* R-spondins are newly recognized players in osteoarthritis that regulate Wnt signaling in osteoblasts. *Arthritis Rheum.* **63**, 3865–3875 (2011).
14. Chaudhuri, J., Chowdhury, D. & Maitra, U. Distinct functions of eukaryotic translation initiation factors eIF1A and eIF3 in the formation of the 40 S ribosomal preinitiation complex. *J. Biol. Chem.* **274**, 17975–17980 (1999).
15. Christianson, J.C. *et al.* Defining human ERAD networks through an integrative mapping strategy. *Nat. Cell Biol.* **14**, 93–105 (2012).
16. Sato, R. *et al.* Ossification of the posterior longitudinal ligament of the cervical spine: histopathological findings around the calcification and ossification front. *J. Neurosurg. Spine* **7**, 174–183 (2007).
17. Zhang, N., Kaur, R., Akhter, S. & Legerski, R.J. Cdc5L interacts with ATR and is required for the S-phase cell-cycle checkpoint. *EMBO Rep.* **10**, 1029–1035 (2009).
18. Ajuh, P. *et al.* Functional analysis of the human CDC5L complex and identification of its components by mass spectrometry. *EMBO J.* **19**, 6569–6581 (2000).
19. Yu, J., Madison, J.M., Mundlos, S., Winston, F. & Olsen, B.R. Characterization of a human homologue of the *Saccharomyces cerevisiae* transcription factor Spt3 (SUPT3H). *Genomics* **53**, 90–96 (1998).
20. Estrada, K. *et al.* Genome-wide meta-analysis identifies 56 bone mineral density loci and reveals 14 loci associated with risk of fracture. *Nat. Genet.* **44**, 491–501 (2012).
21. Karasugi, T. *et al.* A genome-wide sib-pair linkage analysis of ossification of the posterior longitudinal ligament of the spine. *J. Bone Miner. Metab.* **31**, 136–143 (2013).

22. Kawaguchi, H. *et al.* in *OPLL: Ossification of the Posterior Longitudinal Ligament* 2nd edn. (eds. Yonenobu, K., Nakamura, K. & Toyama, Y.) 71–75 (Springer, Tokyo, 2006).
23. Shukunami, C. *et al.* Chondrogenic differentiation of clonal mouse embryonic cell line ATDC5 *in vitro*: differentiation-dependent gene expression of parathyroid hormone (PTH)/PTH-related peptide receptor. *J. Cell Biol.* **133**, 457–468 (1996).
24. FANTOM Consortium and RIKEN PMI and CLST (DGT). A promoter-level mammalian expression atlas. *Nature* **507**, 462–470 (2014).
25. Castleman, V.H. *et al.* Mutations in radial spoke head protein genes *RSPH9* and *RSPH4A* cause primary ciliary dyskinesia with central-microtubular-pair abnormalities. *Am. J. Hum. Genet.* **84**, 197–209 (2009).
26. Huber, C. & Cormier-Daire, V. Ciliary disorder of the skeleton. *Am. J. Med. Genet. C. Semin. Med. Genet.* **160C**, 165–174 (2012).
27. Cornils, H., Kohler, R.S., Hergovich, A. & Hemmings, B.A. Human NDR kinases control G_1/S cell cycle transition by directly regulating p21 stability. *Mol. Cell. Biol.* **31**, 1382–1395 (2011).
28. Harada, Y. *et al.* Osteogenic lineage commitment of mesenchymal stem cells from patients with ossification of the posterior longitudinal ligament. *Biochem. Biophys. Res. Commun.* **443**, 1014–1020 (2014).
29. Yang, T.P. *et al.* Genevar: a database and Java application for the analysis and visualization of SNP-gene associations in eQTL studies. *Bioinformatics* **26**, 2474–2476 (2010).
30. Raychaudhuri, S. *et al.* Identifying relationships among genomic disease regions: predicting genes at pathogenic SNP associations and rare deletions. *PLoS Genet.* **5**, e1000534 (2009).

ONLINE METHODS

Subjects. The characteristics of each case-control group are shown in **Supplementary Table 1**. OPLL was diagnosed by experienced spinal surgeons from the participating hospitals on the basis of radiographic examination of the spine. Ectopic bone formation of the posterior longitudinal ligament in the cervical region of the spine was evaluated. A total of 1,660 Japanese individuals who had OPLL of more than two vertebra segments were included in this study. We used genome-wide screening data from subjects with 1 of 10 diseases (1,145 with cerebral aneurysm, 1,034 with chronic obstructive pulmonary disease, 811 with endometrial cancer, 1,020 with esophageal cancer, 935 with glaucoma, 1,442 with atopic dermatitis, 1,667 with epilepsy, 1,732 with Graves' disease, 612 with nephrotic syndrome and 1,016 with urolithiasis) unrelated to OPLL in the BioBank Japan Project[31], 978 volunteers from the Osaka-Midosuji Rotary Club in Japan and 887 healthy subjects from the PharmaSNP Consortium for the controls. All individuals gave written informed consent to participate in the study. This research project was approved by the ethical committees at the RIKEN Yokohama Institute.

Genotyping and quality control for GWAS. Genomic DNA was extracted from peripheral blood leukocytes using a standard method. For the GWAS, we genotyped case samples using the Illumina HumanOmniExpressExome BeadChip and control samples using the Illumina HumanOmniExpress BeadChip and the Illumina HumanExome BeadChip. After standard SNP quality control, which excluded SNPs with a call rate of <0.99, SNPs that deviated from Hardy-Weinberg equilibrium ($P < 1 \times 10^{-6}$ in controls) and non-polymorphic SNPs, a total of 616,496 autosomal SNPs were used for further analysis. For sample quality control, we evaluated cryptic relatedness for each sample with an identity-by-state method and removed samples that showed second-degrees relatedness or closer. To examine population stratification in this study, we performed PCA[32] using four reference populations from HapMap data as the reference, including Europeans (CEU), Africans (YRI), Japanese (JPT) and Han Chinese (CHB), with smartpca[32]. We generated the scatterplot, using the top two associated principal components (eigenvectors) to identify outliers who did not belong to the JPT/CHB cluster. Subsequently, we performed PCA using only the genotype information from the case and control subjects without HapMap data to further evaluate population substructure. After performing PCA, we selected 1,112 cases and 6,810 controls within the major Japanese (Hondo) cluster for subsequent analysis. We used the quantile-quantile plot of observed P values to evaluate the potential effect of population stratification.

In the replication study, we genotyped 548 individuals with OPLL using a multiplex PCR–based Invader assay (Third Wave Technologies). We recruited 6,469 controls within the Hondo cluster registered in BioBank Japan without OPLL for the replication study. The genotype concordance rate for the six SNPs in **Table 1** between samples genotyped using the Illumina HumanOmniExpressExome BeadChip and the same samples genotyped with the multiplex PCR–based Invader assay was 0.9997.

Statistical analysis. In the GWAS and the replication study, we assessed the association of each SNP with the 1-degree-of-freedom Cochran-Armitage trend test. We calculated OR values and their CIs from a 2 × 2 allele frequency table. We combined data from the GWAS and replication study using the Mantel-Haenszel method and examined heterogeneity between studies using the Breslow-Day test[33]. Regional association plots were generated using LocusZoom[34]. We carried out conditional logistic regression analysis with PLINK v1.07 (ref. 35), adjusting for the top SNPs for each locus to determine whether independently associated SNPs existed.

X-chromosome association study. We performed testing for association on the X chromosome for male and female genotypes separately. For male genotypes, we used 758 cases and 3,988 controls. After quality control as described above, we applied the χ^2 test to the 2 × 2 contingency table for 12,401 SNPs. For female genotypes, we used 354 cases and 2,822 controls and applied the 1-degree-of-freedom Cochran-Armitage trend test for 12,908 SNPs. We combined the male and female association test results for 12,229 SNPs using the inverse normal method[36].

Imputation. We performed genotype imputation within the GWAS using Minimac[37]. We used individuals from the 1000 Genomes Project (phased JPT, CHB and Han Chinese South (CHS) data; March 2012) as reference populations[38]. Because imputation errors are more serious when allele frequencies are low, SNPs with minor allele frequencies of <1% were excluded. SNPs with a low quality of imputation (Minimac software quality score of $R^2 < 0.9$) were also excluded. After quality control, 5,163,786 imputed SNPs were available for analysis. Association tests were performed for dosage with mach2dat[39].

Pathway analysis. We investigated connections between genes in the OPLL-associated loci with GRAIL[30]. We set the parameters as follows: genome assembly, release 22/hg18; HapMap population, JPT + CHB; functional data source, PubMed text (August 2012); gene size correction, off; gene list, all human genes within the database. The rs numbers of the six SNPs listed in **Table 1** were used as a query.

Gene expression analysis. MSCs from the spinal ligaments of individuals with and without OPLL were obtained as previously described[28]. ATDC5 cells (RIKEN Cell Bank) were cultured as previously described[23]. cDNA from MSCs, ATDC5 cells, dermal fibroblast and bone was synthesized for quantitative RT-PCR using the Sensiscript RT kit (Qiagen). Quantitative RT-PCR was performed with a StepOnePlus Real-Time PCR system (Applied Biosystems) using the QuantiTect SYBR Green PCR kit (Qiagen).

Microarray analysis. We analyzed mRNA expression in MSCs from the spinal ligaments of individuals with and without OPLL[28] using the SurePrint G3 Human Gene Expression 8x60K array (Agilent Technologies). For the transcripts whose levels were changed by >2-fold and had a false discovery rate–corrected Welch's t-test P value of <0.05, we verified the difference in expression by qPCR ($n = 8$ for individuals with and without OPLL).

31. Nakamura, Y. The BioBank Japan Project. *Clin. Adv. Hematol. Oncol.* **5**, 696–697 (2007).
32. Price, A.L. *et al.* Principal components analysis corrects for stratification in genome-wide association studies. *Nat. Genet.* **38**, 904–909 (2006).
33. Breslow, N.E. & Day, N.E. Statistical methods in cancer research. Volume II—the design and analysis of cohort studies. *IARC Sci. Publ.* (82), 1–406 (1987).
34. Pruim, R.J. *et al.* LocusZoom: regional visualization of genome-wide association scan results. *Bioinformatics* **26**, 2336–2337 (2010).
35. Purcell, S. *et al.* PLINK: a tool set for whole-genome association and population-based linkage analyses. *Am. J. Hum. Genet.* **81**, 559–575 (2007).
36. Tukiainen, T. *et al.* Chromosome X–wide association study identifies loci for fasting insulin and height and evidence for incomplete dosage compensation. *PLoS Genet.* **10**, e1004127 (2014).
37. Howie, B., Fuchsberger, C., Stephens, M., Marchini, J. & Abecasis, G.R. Fast and accurate genotype imputation in genome-wide association studies through pre-phasing. *Nat. Genet.* **44**, 955–959 (2012).
38. 1000 Genomes Project Consortium. A map of human genome variation from population-scale sequencing. *Nature* **467**, 1061–1073 (2010).
39. Li, Y., Willer, C.J., Ding, J., Scheet, P. & Abecasis, G.R. MaCH: using sequence and genotype data to estimate haplotypes and unobserved genotypes. *Genet. Epidemiol.* **34**, 816–834 (2010).

Skeletal Radiol (2014) 43:1477–1480
DOI 10.1007/s00256-014-1912-8

CASE REPORT

Severe kyphotic deformity resulting from collapses of cemented and adjacent vertebrae following percutaneous vertebroplasty using calcium phosphate cement. A case report

Toshitaka Yoshii · Hiroko Ueki · Tsuyoshi Kato · Shoji Tomizawa · Atsushi Okawa

Received: 3 February 2014 / Revised: 31 March 2014 / Accepted: 8 May 2014 / Published online: 1 June 2014

Abstract Percutaneous vertebroplasty (PVP) has been increasingly performed for the treatment of osteoporotic vertebral compression fracture. Despite its minimally invasive procedure, several complications associated with PVP have been reported, including adjacent-level vertebral fracture. Although rare, recollapse of the same vertebrae after PVP has also been reported. However, previous studies have not described a case in which collapses of both the cemented vertebrae and adjacent-level vertebrae occurred following PVP. Here, we report a rare case of severe kyphotic deformity resulting from collapses at the cemented and adjacent vertebrae after PVP using calcium phosphate cement (CPC). The patient required a highly invasive reconstruction procedure as a salvage surgery.

Keywords Percutaneous vertebroplasty · Calcium phosphate cement · Recollapse · Complication

Introduction

Vertebral compression fractures (VCFs), whether osteoporotic, traumatic, or secondary to other pathological conditions, can be extremely painful and associated with increased morbidity and mortality [1]. Percutaneous vertebroplasty (PVP) or kyphoplasty has been increasingly performed for the treatment of VCFs and pseudoarthrosis [2, 3]. This technique is effective in providing immediate pain reduction and promoting an early return to daily activities. For many years, poly-methyl methacrylate (PMMA) cement has been used in PVP for the augmentation of the vertebrae [4, 5]. Recently, the efficacy of using calcium phosphate cement (CPC) in PVP as a filling material has been reported because of its nontoxic, biocompatible, and osteoconductive properties [6, 7].

The image-guided, minimally invasive PVP procedure offers less risks compared with open surgery [8]. However, several complications associated with PVP have been reported, including pulmonary embolism, neurological deficits, infection, and new VCFs [9–11]. The incidence of new VCFs after PVP has been reported to be 12–52 % [12, 13]. In the previous studies, 41–64 % of the new VCFs occurred at the vertebrae adjacent to the cemented vertebrae [13, 14]. Although rare, recollapse or refracture of the same vertebral body after PVP has also been reported with an incidence of 0.52 % [15]. It is still unclear whether the recollapse after PVP is a natural progression of osteoporosis [16]. However, several risk factors associated with recollapse of the cemented vertebrae have been suggested, including osteonecrosis, cystic filling pattern of cement, preoperative kyphotic angle, and its correction [15, 17].

Although both the recollapse of the cemented vertebrae and adjacent-level fracture are clinically recognized complications after PVP, to our knowledge, previous reports have not described a case in which collapses of both the cemented vertebrae and adjacent-level vertebrae occurred in the same patient. Here, we report a rare case of serial vertebral collapses of the augmented and adjacent vertebrae after PVP using CPC, resulting in extremely severe kyphotic deformity of the spine (regional kyphosis >75 degrees). The patient required anterior-posterior combined reconstruction to restore the spinal sagittal alignment.

Toshitaka Yoshii and Hiroko Ueki contributed equally to this study.

T. Yoshii (✉) · H. Ueki · T. Kato · S. Tomizawa · A. Okawa
Department of Orthopaedic and Spinal Surgery, Graduate School, Tokyo Medical and Dental University, 1-5-45 Yushima,, Bunkyo-ku, Tokyo 113-8519, Japan
e-mail: yoshii.orth@tmd.ac.jp

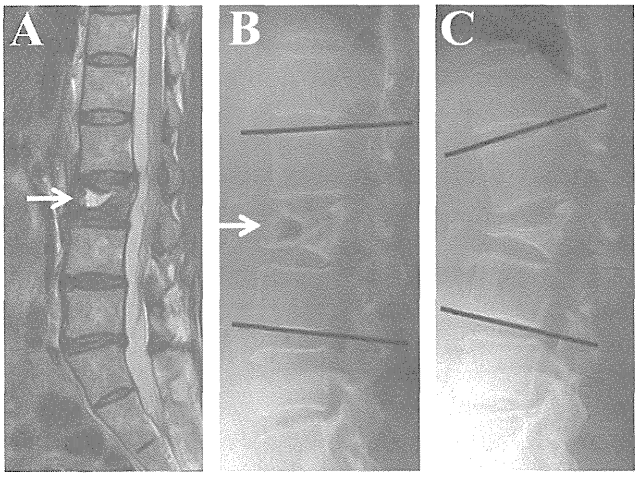

Fig. 1 Preoperative magnetic resonance imaging (**a**). Preoperative lateral X-rays in supine position (**b**) and standing position (**c**). The *white arrows* indicate the cleft in the L3 vertebrae

Case presentation

A 74-year-old woman suffered from low back pain without a history of trauma and visited our clinic in October of 2010. Radiological studies demonstrated an L3 osteoporotic VCF. Although she was conservatively treated with a lumbar spine brace for 3 months, her back pain persisted. The patient was admitted to our hospital. There were no neurological deficits. However, her visual analog scale (VAS) score for low back pain was 10 points (full score: 10 points). The patient's comorbidities included a history of deep vein thrombosis, anemia, and osteoporosis. Her bone mineral density measured at the proximal femur was 0.566 g/cm^2 (T score: −3.1, Z score: −0.6). Magnetic resonance imaging (MRI) demonstrated cleft with fluid collection in the L3 vertebrae (Fig. 1a), and the X-ray in the supine position demonstrated a vacuum phenomenon in the L3 vertebrae (Fig. 1b). Additionally, functional X-rays revealed instability of the vertebrae; the patient was diagnosed pseudoarthrosis of L3. The regional kyphotic angle at L2-4 in the standing X-ray was 40 degrees (Fig. 1c). Her standing X-ray of the total spine revealed a kyphotic sagittal alignment; the sagittal vertical axis (SVA) was 156 mm.

Three months after the symptom onset, the patient underwent a PVP using CPC under local anesthesia using an endoscopic technique [18]. Fifteen milliliters of CPC was injected using a transpedicular approach under local anesthesia after debridement of the intravertebral scar was performed under endoscopy. Since the mechanical strength of CPC reaches its maximum in approximately 24 h, the patient needed bed rest for 24 h after PVP under hospitalization. She started walking 1 day after the surgery with a hard corset. Her back pain immediately resolved; the VAS score was improved from 10 to 2.2 points. The postoperative kyphotic angle at L2-4 and the SVA were improved to 2 degrees and 75 mm, respectively.

The post-operative X-ray demonstrated an acceptable reduction of the vertebra without CPC leakage or collapse (Fig. 2a). One month after the PVP, her low back pain gradually increased again. A routine X-ray at 1 month revealed recollapse of the L3 vertebrae and fracture of the CPC without any events of trauma (Fig. 2b). Two months after the PVP, a regional kyphotic change developed at the level of the L3 vertebrae (L2-4: 24 degree kyphosis). Subsequently, an adjacent-level VCF (L4) occurred, resulting in further severe kyphotic deformity (L2-4: 77 degree kyphosis, SVA: over 250 mm, Fig. 2c).

The patient underwent anterior-posterior combined reconstructive surgery at 6 months after the initial PVP (Fig. 2d). The sagittal spine alignment was successfully restored after the surgery; the SVA at standing X-ray was 65 mm. The patient was discharged from the hospital with an independent gait. The spinal alignment was maintained at the 1-year follow-up.

Discussion

PVP is traditionally performed using PMMA [4, 5]; however, PMMA lacks the potential for osteoconduction,

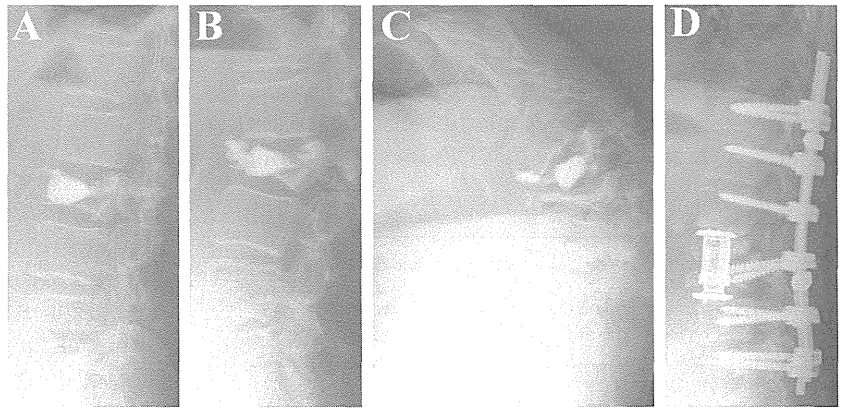

Fig. 2 Lateral X-rays immediately after vertebroplasty (**a**), 1 month (**b**), and 6 months after vertebroplasty using CPC (**c**). Lateral X-ray after the reconstruction surgery (**d**)

osteoinduction, remodeling, or integration into the adjacent bone. Additionally, there are thermal effects during polymerization, which is potentially harmful for both inside and outside the vertebrae [5]. Therefore, CPC has gained recent interest as a filling material for PVP because of its nontoxic, biocompatible, and osteoconductive properties [5, 7]. Various studies have reported the clinical efficacy of PVP using CPC for the treatment of osteoporotic VCFs [6, 18]. The compressive strength of CPC is known to be less than that of normal cortical bone and greater than that of cancellous bone. However, the mechanical properties of CPC are inferior to those of PMMA [19, 20]. Furthermore, the strength can be reduced when CPC is mixed with blood [21]. Therefore, there is a potential risk for the fracture of CPC and the collapse of the augmented vertebral body after PVP [22].

In this case report, PVP using CPC was performed for the treatment of L3 VCF. We used an endoscopic technique for the debridement of the intravertebral scar [18]. Although the augmentation of the L3 vertebrae and pain relief were successfully achieved, the fragmentation of CPC and the recollapse of the augmented vertebrae occurred 1 month after the surgery. The endoscopic technique is useful to remove the granulation tissue in the vertebrae and to sufficiently fill CPC in the cavity [18]. However, too much debridement may cause violation of the surrounding cancellous bone and weaken its mechanical strength. Furthermore, Blattert et al. has reported that the mechanical property of CPC is particularly weak in flexural strength: there is a tenfold difference in flexural strength between CPC (3 Mpa) and PMMA (30 Mpa) [19]. Therefore, CPC is susceptible to failure in situations where flexural, tractive, and/or shear forces can act on the filling material. As previously described, the use of CPC in PVP may not be suitable for the treatment of burst-type fractures, flexion-distraction injuries, or rotational instable fractures [23, 24]. The original VCF in this case was classified as an incomplete burst-type [25], and there was significant instability in the fractured vertebrae in the functional X-ray. For such cases, use of stiffer filling material, such as PMMA, or PVP with posterior pedicle screw instrumentation would be better to prevent the recollapse of the augmented vertebrae [26, 27].

Previous studies have investigated risk factors for recollapse of the cemented vertebrae after PVP. Kang et al. has reported that preoperative kyphotic angle significantly influences the occurrence of the recollapse of the vertebrae augmented by cement. Chen et al. have also shown several risk factors for the recollapse, including greater anterior vertebral height restoration and cystic filling pattern [15, 17]. In the presented case, preoperative hyperkyphosis at the fractured vertebrae needed great anterior vertebral height restoration using a large amount of CPC with cystic filling pattern. In addition to the mechanical weakness of CPC, these factors may have caused the recollapse of the cemented vertebrae after PVP.

Adjacent-level VCF is also known as one of the complications associated with PVP. Although it remains unclear whether PVP directly causes adjacent vertebral fractures, the relative risk of adjacent-level fractures has been reported to be 4.62 times that for nonadjacent level fracture after PVP [13]. Biomechanical studies have shown that the volume of cement is associated with the subsequent adjacent level VCF [28, 29]. When a large volume of bone cement is injected into a vertebral body, the level of stiffness exceeds that of normal bone [29]. In the case presented here, the large amount of cement (nearly 15 ml) needed to be injected because of the large space of cleft in the fractured vertebrae. This can be considered as one of the causes of subsequent adjacent-level fracture. Furthermore, it is known that sagittal balance and focal kyphosis has been considered a risk factor for additional spine fractures [30]. Therefore, recollapse of the augmented vertebrae and resulting kyphosis can be a risk factor for the new adjacent-level VCF after PVP. Indeed, in this case, the events of CPC fragmentation, recollapse of the cemented vertebrae, regional kyphotic change, and further adjacent-level fracture were serially observed. As a result, the collapses of two adjacent vertebrae (L3 and L4) lead to extremely severe kyphosis and instability of the spine.

Several salvage procedures for failed PVP have been reported, including repeated PVP, anterior fusion, posterior fusion, and anterior-posterior combined reconstruction [31]. Repeated PVP is difficult to perform for the highly collapsed vertebrae, and it is impossible to correct the severe kyphotic deformity. Thus, we chose reconstruction salvage surgery for this patient. The anterior-posterior combined reconstruction procedure was effective to correct the severe kyphotic deformity and maintain the sagittal alignment.

Conclusions

PVP is an effective minimally invasive procedure for the treatment of osteoporotic VCF in the elderly. CPC is an attractive filling material for PVP because of its biocompatibility and osteoconductivity. However, in cases with highly unstable VCF, PVP using CPC can result in recollapse of the augmented vertebrae and severe kyphotic deformity, which may require highly invasive reconstruction procedure as a salvage surgery.

Informed consent Written informed consent was obtained from the patient for publication of this case report and any accompanying images.

Conflict of interest The authors declare that they have no conflicts of interest.

References

1. Bliuc D, Nguyen ND, Milch VE, Nguyen TV, Eisman JA, Center JR. Mortality risk associated with low-trauma osteoporotic fracture and subsequent fracture in men and women. JAMA. 2009;301:513–21.
2. Hulme PA, Krebs J, Ferguson SJ, Berlemann U. Vertebroplasty and kyphoplasty: a systematic review of 69 clinical studies. Spine. 2006;31:1983–2001. Phila Pa 1976.
3. Ploeg WT, Veldhuizen AG, The B, Sietsma MS. Percutaneous vertebroplasty as a treatment for osteoporotic vertebral compression fractures: a systematic review. Eur Spine J. 2006;15:1749–58.
4. Garfin SR, Yuan HA, Reiley MA. New technologies in spine: kyphoplasty and vertebroplasty for the treatment of painful osteoporotic compression fractures. Spine. 2001;26:1511–5. Phila Pa 1976.
5. Lieberman IH, Togawa D, Kayanja MM. Vertebroplasty and kyphoplasty: filler materials. Spine J. 2005;5:305S–16.
6. Nakano M, Hirano N, Ishihara H, Kawaguchi Y, Watanabe H, Matsuura K. Calcium phosphate cement-based vertebroplasty compared with conservative treatment for osteoporotic compression fractures: a matched case–control study. J Neurosurg Spine. 2006;4:110–7.
7. Turner TM, Urban RM, Singh K, Hall DJ, Renner SM, Lim TH, et al. Vertebroplasty comparing injectable calcium phosphate cement compared with polymethylmethacrylate in a unique canine vertebral body large defect model. Spine J. 2008;8:482–7.
8. Jensen ME, Evans AJ, Mathis JM, Kallmes DF, Cloft HJ, Dion JE. Percutaneous polymethylmethacrylate vertebroplasty in the treatment of osteoporotic vertebral body compression fractures: technical aspects. AJNR Am J Neuroradiol. 1997;18:1897–904.
9. Cosar M, Sasani M, Oktenoglu T, Kaner T, Ercelen O, Kose KC, et al. The major complications of transpedicular vertebroplasty. J Neurosurg Spine. 2009;11:607–13.
10. Zhang JD, Poffyn B, Sys G, Uyttendaele D. Comparison of vertebroplasty and kyphoplasty for complications. Orthop Surg. 2011;3:158–60.
11. Eom KS, Kim TY. Percutaneous vertebroplasty-induced adjacent vertebral compression fracture. Pain Physician. 2012;15:E527–32.
12. Ahn Y, Lee JH, Lee HY, Lee SH, Keem SH. Predictive factors for subsequent vertebral fracture after percutaneous vertebroplasty. J Neurosurg Spine. 2008;9:129–36.
13. Trout AT, Kallmes DF, Kaufmann TJ. New fractures after vertebroplasty: adjacent fractures occur significantly sooner. AJNR Am J Neuroradiol. 2006;27:217–23.
14. Li YA, Lin CL, Chang MC, Liu CL, Chen TH, Lai SC. Subsequent vertebral fracture after vertebroplasty: incidence and analysis of risk factors. Spine. 2012;37:179–83. Phila Pa 1976.
15. Chen LH, Hsieh MK, Liao JC, Lai PL, Niu CC, Fu TS, et al. Repeated percutaneous vertebroplasty for refracture of cemented vertebrae. Arch Orthop Trauma Surg. 2011;131:927–33.
16. Kallmes DF, Jensen ME. Percutaneous vertebroplasty. Radiology. 2003;229:27–36.
17. Kang SK, Lee CW, Park NK, Kang TW, Lim JW, Cha KY, et al. Predictive risk factors for refracture after percutaneous vertebroplasty. Ann Rehabil Med. 2011;35:844–51.
18. Hoshino M, Nakamura H, Konishi S, Nagayama R, Terai H, Tsujio T, et al. Endoscopic vertebroplasty for the treatment of chronic vertebral compression fracture. Technical note. J Neurosurg Spine. 2006;5:461–7.
19. Blattert TR, Jestaedt L, Weckbach A. Suitability of a calcium phosphate cement in osteoporotic vertebral body fracture augmentation: a controlled, randomized, clinical trial of balloon kyphoplasty comparing calcium phosphate versus polymethylmethacrylate. Spine. 2009;34:108–14. Phila Pa 1976.
20. Tomita S, Molloy S, Jasper LE, Abe M, Belkoff SM. Biomechanical comparison of kyphoplasty with different bone cements. Spine. 2004;29:1203–7. Phila Pa 1976.
21. Shiga Y, Shimogoryo R, Oka T, Matsuya S, Ishikawa K. The effects of initial hemostatic period on the mechanical strength and transformation of apatite cement. Dent Mater J. 2004;23:335–9.
22. Piazzolla A, De Giorgi G, Solarino G. Vertebral body recollapse without trauma after kyphoplasty with calcium phosphate cement. Musculoskelet Surg. 2011;95:141–5.
23. Schmelzer-Schmied N, Cartens C, Meeder PJ, Dafonseca K. Comparison of kyphoplasty with use of a calcium phosphate cement and non-operative therapy in patients with traumatic non-osteoporotic vertebral fractures. Eur Spine J. 2009;18:624–9.
24. Robinson Y, Heyde CE, Forsth P, Olerud C. Kyphoplasty in osteoporotic vertebral compression fractures–guidelines and technical considerations. J Orthop Surg Res. 2011;6:43.
25. Magerl F, Aebi M, Gertzbein SD, Harms J, Nazarian S. A comprehensive classification of thoracic and lumbar injuries. Eur Spine J. 1994;3:184–201.
26. Shen YX, Zhang P, Zhao JG, Xu W, Fan ZH, Lu ZF, et al. Pedicle screw instrumentation plus augmentation vertebroplasty using calcium sulfate for thoracolumbar burst fractures without neurologic deficits. Orthop Surg. 2011;3:1–6.
27. Zhang L, Zou J, Gan M, Shi J, Li J, Yang H. Treatment of thoracolumbar burst fractures: short-segment pedicle instrumentation versus kyphoplasty. Acta Orthop Belg. 2013;79:718–25.
28. Liebschner MA, Rosenberg WS, Keaveny TM. Effects of bone cement volume and distribution on vertebral stiffness after vertebroplasty. Spine. 2001;26:1547–54. Phila Pa 1976.
29. Kim JM, Shin DA, Byun DH, Kim HS, Kim S, Kim HI. Effect of bone cement volume and stiffness on occurrences of adjacent vertebral fractures after vertebroplasty. J Korean Neurosurg Soc. 2012;52:435–40.
30. Kayanja MM, Togawa D, Lieberman IH. Biomechanical changes after the augmentation of experimental osteoporotic vertebral compression fractures in the cadaveric thoracic spine. Spine J. 2005;5:55–63.
31. Yang SC, Chen WJ, Yu SW, Tu YK, Kao YH, Chung KC. Revision strategies for complications and failure of vertebroplasties. Eur Spine J. 2008;17:982–8.

J Neurosurg Spine 21:292–295, 2014

Spinal deformity caused by hyperimmunoglobulin E syndrome

Case report

*Naoko Araya, M.D., Hiroyuki Inose, M.D., Ph.D., Tsuyoshi Kato, M.D., Ph.D., Masanori Saito, M.D., Satoshi Sumiya, M.D., Tsuyoshi Yamada, M.D., Toshitaka Yoshii, M.D., Ph.D., Shigenori Kawabata, M.D., Ph.D., and Atsushi Okawa, M.D., Ph.D.

Department of Orthopaedics, Tokyo Medical and Dental University, Tokyo, Japan

Hyperimmunoglobulin E syndrome (HIES) is a rare primary immunodeficiency syndrome characterized by recurrent staphylococcal infections in the skin and lungs, with an incidence of less than one case per million persons. Skeletal and connective tissue abnormalities, such as scoliosis, osteoporosis, pathological fractures, and hyperextensive joints, are other manifestations of HIES. However, only one report documents the use of implants to treat spinal deformity caused by HIES, which was discovered following corrective surgery resulting in postoperative infection. In this case report, the authors describe a 16-year-old male with low-back pain and infections of the soft tissue. Radiological findings showed deteriorated kyphotic deformity due to the pathological compression fracture of T-11 with intensive conservative treatment. Anterior and posterior fixation surgery was performed. Thereafter, the patient showed no signs of infection. An investigation was conducted to avoid any postoperative infection.
(http://thejns.org/doi/abs/10.3171/2014.4.SPINE13629)

Key Words • **Hyper IgE syndrome** • **Job's syndrome** • **osteoporosis** • **spinal deformity** • **immunodeficiency** • **infection**

Hyperimmunoglobulin E syndrome (HIES) was first reported as Job's syndrome in 1966 by Davis;[1] it was characterized by elevated serum levels of IgE, chronic eczemas, and recurrent respiratory and soft tissue infections.[11] Recently, the cause of HIES was identified as a genetic mutation of *STAT3* and *TYK2*.[11] Symptoms can include not only immune system abnormalities, but also skeletal and connective tissue abnormalities, such as scoliosis, osteoporosis, pathological fractures, and hyperextensive joints.[11] To date, however, only one report has documented scoliosis caused by HIES, which was discovered following corrective surgery that had resulted in postoperative infection.[13] To our knowledge, the present report is the first on the surgical treatment of spinal deformity caused by HIES, which was diagnosed presurgery. Here we describe the case of a surgically treated spinal deformity caused by HIES and discuss various perioperative prophylaxes for preventing postoperative infections in patients with HIES.

Abbreviations used in this paper: BMD = bone mineral density; HIES = hyperimmunoglobulin E syndrome.

* Drs. Araya and Inose contributed equally to this work.

Case Report

History and Examination. A 16-year-old male reported back pain with no evidence of trauma. He visited a nearby hospital, but an examination did not show anything out of the ordinary at that time. Two months later, his back pain continued to worsen. He underwent plain radiography and MRI, and a T-11 compression fracture was diagnosed (Fig. 1). He was then hospitalized at the previous institution for further examination and treated with absolute bed rest. A PET-CT there revealed pathological FDG uptake in the lung, upper jaw, left hip, and T-11 vertebral body (Fig. 2). Because tumor metastasis was suspected, a biopsy of the left hip mass was performed and revealed an infection of *Staphylococcus aureus*. Hyperimmunoglobulin E syndrome was diagnosed because of the elevated serum levels of IgE (Table 1), soft tissue infection, and lung abscess.

The patient was transferred to our hospital where we applied a hard brace to immobilize the fracture. His

This article contains some figures that are displayed in color online but in black-and-white in the print edition.

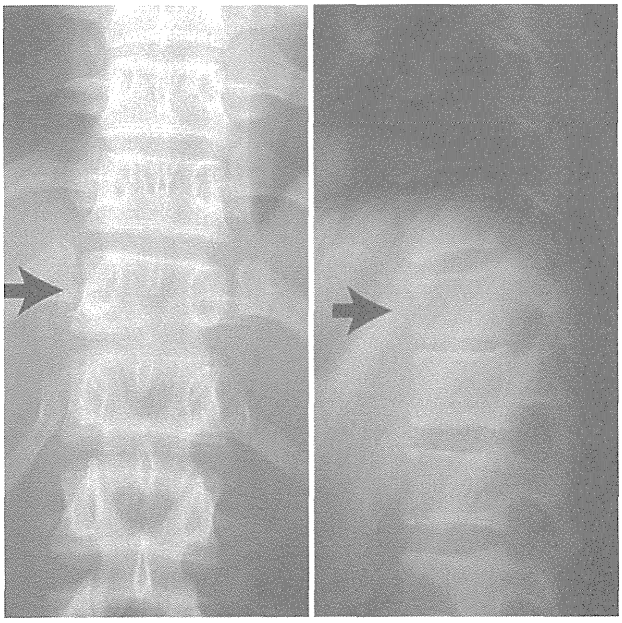

FIG. 1. Plain radiographs showing a compression fracture of T-11 *(arrows)*.

medical history revealed that he had experienced a recurrent surgical site infection when he underwent an Ilizarov surgery for Blount's disease. Genetic investigation to confirm the diagnosis revealed a mutation in *STAT3*. During the radiographic examination, it was discovered that the spinal deformity caused by the compression fracture had rapidly become worse, with a local Cobb angle (T10–12) of 50° (Fig. 3). To avoid the possibility of infection, we performed a spine biopsy as a safety measure. Pathologically, the specimen did not show signs of active inflammation. Additionally, the culture was negative. Thus, we concluded that the compression fracture was caused by bone fragility from the HIES, not by the infection. Even after intensive conservative treatment, his low-back pain continued and

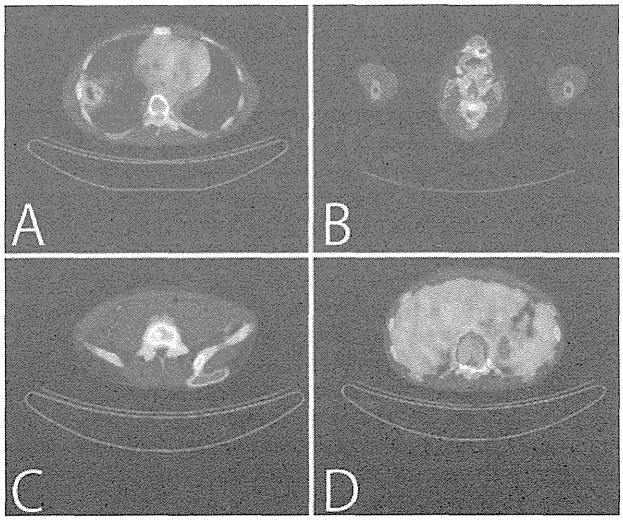

FIG. 2. PET-CT scans showing pathological FDG uptake in the lung **(A)**, upper jaw **(B)**, left hip **(C)**, and T-11 vertebral body **(D)**.

TABLE 1: Preoperative laboratory data*

Variable	Our Patient	Reference Range
WBC (cells/ml)	9400	3600–9300
hemoglobin (g/dl)	9.0	13.8–16.9
CRP (mg/dl)	9.57	<0.3
IgG (mg/dl)	2168	868–1780
IgA (mg/dl)	378	122–412
IgM (mg/dl)	292	28–177
IgE (IU/ml)	3188	<173
bone alkaline phosphatase (μg/L)	15.3	3.7–20.9
deoxypyridinoline (nmol/mmol × creatinine)	15.9	2.1–5.4
BMD (% of young adult mean)	88	

* CRP = C-reactive protein; WBC = white blood cell.

the kyphosis became worse. The pain and deformity made him a suitable candidate for reconstructive surgery. Therefore, we asked the patient and his family if he was willing to treat the kyphosis with surgery, since he had an immune deficiency. They consented, even though they realized the high risk of postoperative infection.

Operation. We performed an anterior and posterior reconstruction and fusion surgery. At first, the lesion was approached through a standard posterolateral thoracotomy over the superior edge of the ninth rib. We performed two discectomies (T10–11, T11–12), a partial corpectomy of T-11, and positioning of a left fibula and rib graft. Then, after moving the patient into the prone position, we proceeded to perform the T9–L1 posterior fusion using pedicle screws. As a result, the postoperative kyphosis Cobb angle was improved to 10° (Fig. 4).

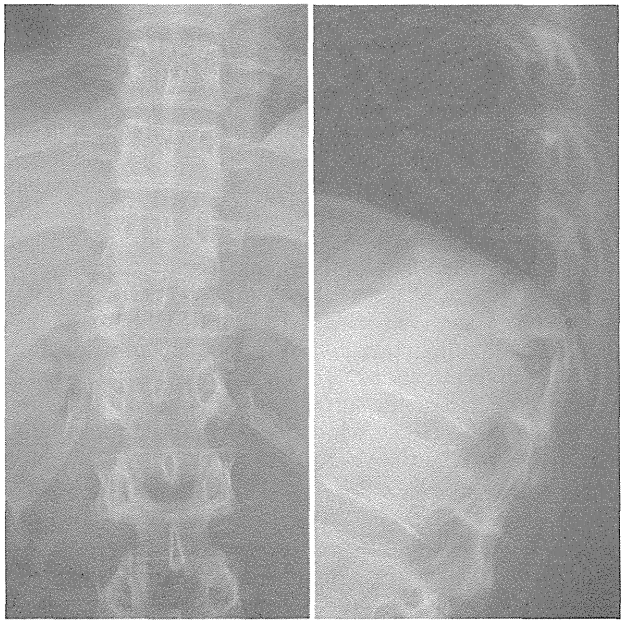

FIG. 3. Plain radiographs showing deteriorated local kyphosis (Cobb angle 50°).

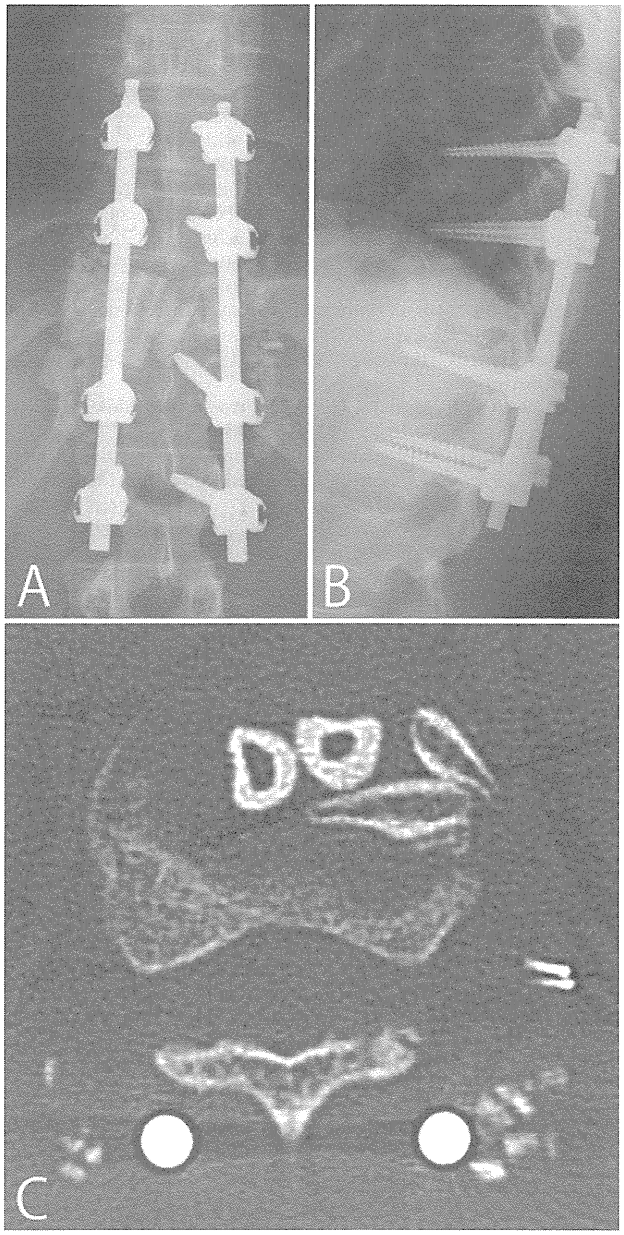

FIG. 4. Postoperative plain radiographs **(A and B)** showing improved local kyphosis (Cobb angle 10°). Axial CT image **(C)** showing the position of the rib and fibula graft positioned in the patient.

To reduce the risk of infection, 4 days prior to surgery we prepared the patient by administering intravenous Ig. On the day of surgery, we administered vancomycin at 8-hour intervals. We also gave him itraconazole orally as a precautionary measure against fungal infection. For treatment of the lung abscess, we continued the administration of trimethoprim/sulfamethoxazole and ampicillin/sulbactam. The latter combination was switched to cefaclor given the improvement of his lung abscess 10 days postoperation.

Postoperative Course. He was discharged 3 weeks after the surgery without any signs of infection and back pain. At his most recent follow-up 15 months after surgery, he showed no signs of surgical site infection, which was confirmed by stable, normal C-reactive protein levels and erythrocyte sedimentation rate levels (Table 2). While the patient's back pain was resolved, a slight loss of reduction in kyphosis Cobb angle was observed on plain radiographs (Fig. 5).

TABLE 2: Postoperative laboratory data*

Parameter	Postop Month					Reference Range
	1	3	6	12	15	
CRP (mg/dl)	<0.03	0.54	<0.03	0.02	0.03	<0.3
ESR (mm/hr)	5	8	2	0	3	<15

* CRP = C-reactive protein; ESR = erythrocyte sedimentation rate.

Discussion

Hyperimmunoglobulin E syndrome is a rare primary immunodeficiency disorder that can also be characterized by skeletal abnormalities, with an incidence of less than 1 case per million persons.[5] Recurrent pathological fractures are noted in more than 50% of patients with HIES.[5] Typically, long bones are affected,[8] and the vertebral column can also be involved.[4] Interestingly, bone mineral density (BMD) is not always a good predictive factor for these pathological fractures. Indeed, the patient in our case appeared to have high bone resorption activity given the elevated urine levels of deoxypyridinoline, but his BMD was within the normal range (Table 1). Hyperimmunoglobulin E syndrome can also cause scoliosis, although the precise mechanisms are yet to be identified.[11]

The surgical indication for juvenile kyphosis has not yet been well established. Opinions are divided regarding

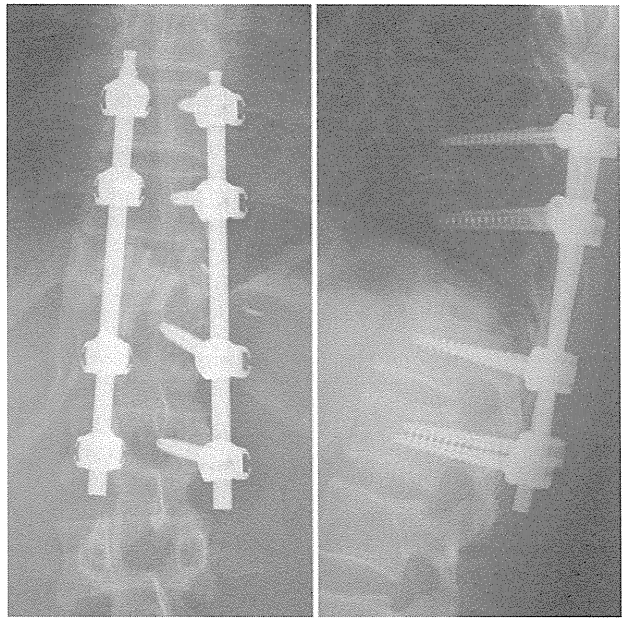

FIG. 5. Postoperative (15 months) plain radiographs showing a slight loss of reduction in local kyphosis.

the application of surgical and nonsurgical procedures in the treatment of juvenile kyphosis.[6,10] As a result, a decision for surgical intervention is an individual one between surgeons and their patients.[14] Recently, increasing sagittal plane deformity has been reported to have a significant impact on health-related quality of life, especially in pain and self image.[9,12] In our case, continuous pain and deteriorating severe local kyphosis led us to consider performing reconstructive surgery.

Indeed, there is much to consider in terms of preventing postoperative infection in patients with HIES.[13] After reviewing the featured case and considering the patient's current status and medical history along with other cases of HIES, we applied preventive measures in the form of antibiotic administration. Because of his lung abscess, the patient was given ampicillin/sulbactam, trimethoprim/sulfamethoxazole, and cefaclor. Additionally, vancomycin was administered right before and the day after surgery to prevent the occurrence of infections of methicillin-resistant *Staphylococcus aureus*, given the patient's long use of various antibiotics.

We also administered intravenous Ig as an immunoprophylaxis, since some reports have documented the usefulness of intravenous Ig for the control of infection with HIES.[2,3,7]

Conclusions

In summary, the success of the patient's spinal surgery was largely attributable to actions we took to avoid infections through the use of various appropriate antibiotics and the administration of intravenous Ig. We must consider the possibility of HIES in juvenile spinal deformity cases, taking into account that these patients have an immune deficiency.

Disclosure

The authors report no conflict of interest concerning the materials or methods used in this study or the findings specified in this paper.

Author contributions to the study and manuscript preparation include the following. Conception and design: Inose. Acquisition of data: Inose. Analysis and interpretation of data: Inose. Drafting the article: Inose, Araya. Critically revising the article: all authors. Reviewed submitted version of manuscript: all authors. Approved the final version of the manuscript on behalf of all authors: Inose.

References

1. Davis SD, Schaller J, Wedgwood RJ: Job's Syndrome. Recurrent, "cold", staphylococcal abscesses. **Lancet 1:**1013–1015, 1966
2. Dreskin SC, Goldsmith PK, Gallin JI: Immunoglobulins in the hyperimmunoglobulin E and recurrent infection (Job's) syndrome. Deficiency of anti-Staphylococcus aureus immunoglobulin A. **J Clin Invest 75:**26–34, 1985
3. Gipponi M, Canova G, Bonalumi U, Bertoglio S, Corbetta G, Sguotti C, et al: Immunoprophylaxis in "septic risk" patients undergoing surgery for gastrointestinal cancer. Results of a randomized, multicenter clinical trial. **Int Surg 78:**63–67, 1993
4. Grimbacher B, Holland SM, Gallin JI, Greenberg F, Hill SC, Malech HL, et al: Hyper-IgE syndrome with recurrent infections—an autosomal dominant multisystem disorder. **N Engl J Med 340:**692–702, 1999
5. Grimbacher B, Holland SM, Puck JM: Hyper-IgE syndromes. **Immunol Rev 203:**244–250, 2005
6. Gutowski WT, Renshaw TS: Orthotic results in adolescent kyphosis. **Spine (Phila Pa 1976) 13:**485–489, 1988
7. Kimata H: High-dose intravenous gamma-globulin treatment for hyperimmunoglobulinemia E syndrome. **J Allergy Clin Immunol 95:**771–774, 1995
8. Kirchner SG, Sivit CJ, Wright PF: Hyperimmunoglobulinemia E syndrome: association with osteoporosis and recurrent fractures. **Radiology 156:**362, 1985
9. Lonner B, Yoo A, Terran JS, Sponseller P, Samdani A, Betz R, et al: Effect of spinal deformity on adolescent quality of life comparison of operative Scheuermann's kyphosis, adolescent idiopathic scoliosis, and normal controls. **Spine (Phila Pa 1976) 38:**1049–1055, 2013
10. Lowe TG, Kasten MD: An analysis of sagittal curves and balance after Cotrel-Dubousset instrumentation for kyphosis secondary to Scheuermann's disease. A review of 32 patients. **Spine (Phila Pa 1976) 19:**1680–1685, 1994
11. Minegishi Y: Hyper-IgE syndrome. **Curr Opin Immunol 21:** 487–492, 2009
12. Petcharaporn M, Pawelek J, Bastrom T, Lonner B, Newton PO: The relationship between thoracic hyperkyphosis and the Scoliosis Research Society outcomes instrument. **Spine (Phila Pa 1976) 32:**2226–2231, 2007
13. Tan WM, Kandiah DA, Tan SB: Hyperimmunoglobulin E syndrome (job syndrome) discovered in a patient following corrective spine surgery: case report and review of the literature. **Spine (Phila Pa 1976) 31:**E471–E474, 2006
14. Wenger DR, Frick SL: Scheuermann kyphosis. **Spine (Phila Pa 1976) 24:**2630–2639, 1999

Manuscript submitted July 3, 2013.
Accepted April 17, 2014.
Please include this information when citing this paper: published online May 16, 2014; DOI: 10.3171/2014.4.SPINE13629.
Address correspondence to: Hiroyuki Inose, M.D., Ph.D., Department of Orthopaedics, Tokyo Medical and Dental University, 1-5-45, Yushima, Bunkyo-ku, Tokyo, Japan, 108-0075. email: inoorth@tmd.ac.jp.